Exploring the 1,3-Benzoxazine Chemotype for Cannabinoid Receptor 2 as a Promising Anti-Cancer Therapeutic

*Nicola Gambacorta,[a#] Valeria Gasperi,[b#] Tatiana Guzzo,[c#] Francesco Saverio Di Leva,[d] Fulvio Ciriaco,[e] Cristina Sánchez,[f] Valentina Tullio,[b] Diego Rozzi,[c] Luciana Marinelli,[d] Alessandra Topai,[*c] Orazio Nicolotti[*a] and Mauro Maccarrone[*g,h]*

[a] Department of Pharmacy-Pharmaceutical Sciences, University of the Studies of Bari "Aldo Moro", Via E. Orabona 4, 70125, Bari, Italy;

[b] Department of Experimental Medicine, Tor Vergata University of Rome, Via Montpellier 1, 00133, Rome, Italy;

[c] C4T S.r.l Colosseum Combinatorial Chemistry Centre for Technology, Via della Ricerca Scientifica snc, 00133, Rome, Italy;

[d] Department of Pharmacy, University of Naples Federico II, 80131 Via D. Montesano 49, 80131, Naples, Italy;

[e] Department of Chemistry, University of the Studies of Bari "Aldo Moro", Via E. Orabona 4, 70125, Bari, Italy ;

[f] Department of Biochemistry and Molecular Biology, School of Biology, Complutense University, C/ José Antonio Nováis, 12, 28040, Madrid, Spain;

[g] Department of Biotechnological and Applied Clinical Sciences, University of L'Aquila, Via Vetoio, 67100, Coppito, L'Aquila, Italy;

[h] European Center for Brain Research/Santa Lucia Foundation IRCCS, Via del Fosso di Fiorano 64, 00143, Rome, Italy.

[#] These authors contributed equally to the manuscript.

* Corresponding authors

26 KEYWORDS

27 1,3-benzoxazin-4-one, inflammation, cancer, CB_2, neurodegenerative disorders, neuropathic pain.

ABSTRACT

The discovery of selective agonists of cannabinoid receptor 2 (CB_2) is strongly pursued to successfully tuning endocannabinoid signaling for therapeutic purposes. However, the design of selective CB_2 agonists is still challenging because of the high homology with the cannabinoid receptor 1 (CB_1) and for the yet unclear molecular basis of the agonist/antagonist switch. Here, the 1,3-benzoxazine scaffold is presented as a versatile chemotype for the design of CB_2 agonists from which 25 derivatives were synthesized. Among these, compound **7b5** (CB_2 EC_{50} = 110 nM, CB_1 EC_{50} > 10 μM) demonstrated to impair proliferation of triple negative breast cancer BT549 cells and to attenuate the release of pro-inflammatory cytokines in a CB_2-dependent manner. Furthermore, **7b5** abrogated the activation of extracellular signal-regulated kinase (ERK) 1/2, a key pro-inflammatory and oncogenic enzyme. Finally, molecular dynamics studies suggested a new rationale for the *in vitro* measured selectivity and for the observed agonist behavior.

INTRODUCTION

Cannabinoid receptors 1 and 2 (CB_1 and CB_2) are G protein-coupled receptors discovered more than 30 years ago [1–3] as molecular targets of Δ^9-tetrahydrocannabinol (Δ^9-THC), the main psychoactive component of *Cannabis sativa* [4]. Since its discovery, CB_1 has been recognized as an important pharmacological target for several pathological conditions affecting either the central nervous system (CNS) [5,6], where it is highly present, or peripheral districts, where it is equally active [7,8]. Nevertheless, research aimed at identifying selective CB_1 agonists/antagonists for therapeutic purposes has suffered a sudden halt due to the severe psychomimetic side effects [9]. At the same time, intensive investigations on CB_2 have witnessed a strong acceleration, especially thanks to the development of more sophisticated methods demonstrating that this receptor is not exclusively expressed in immune cells and organs, as originally assumed [10], but is also present in heart [11], gastrointestinal tract [12], endothelium [13], kidney [14] , adipose tissue [15] , skin [16] and bones[17] . Importantly, it is now acknowledged that CB_2 is also expressed in the brain, where it regulates not only the activity of microglia [18] but also that of astrocytes and neurons [19–22]. The rational design of selective CB_2 agonists as therapeutic tools for multiple pathological conditions opens new opportunities, especially for the lack of psychotropic effects associated with receptor activation. For example, CB_2 targeting is a promising strategy for the management of inflammatory degenerative musculoskeletal diseases, such as osteoarthritis [23], and of pathologies characterized by impairment of bone remodeling, including coeliac disease-related bone loss [24] as well as breast cancer-induced bone resorption [25]. Consistent with a significant gain of expression in human cancer biopsies, CB_2 also correlates with tumor aggressiveness and poor prognosis [26–28] and its pharmacological modulation may result in anti-tumor effects, including inhibition of proliferation, induction of cell death, and decrease in angiogenesis and metastasis [26,28–31]. Additionally, CB_2 counteracts the self-sustaining cycle of neuroinflammation and/or neurodegeneration usually associated with neurodegenerative pathologies. Accordingly, CB_2 activation has been proved to dampen microglial-

mediated inflammation, while CB_2 genetic ablation leads to exacerbation of pro-inflammatory microglial behaviors [2,32]. Likewise, pharmacological CB_2 stimulation displayed protective effects against a plethora of neurodegenerative diseases, such as Alzheimer's disease (by reducing amyloid-β overload, promoting neurogenesis, and ameliorating cognitive impairment) [33–36], Parkinson's disease (by reducing astrocyte and microglia activation, macrophage infiltration and neuron death) [37,38], multiple sclerosis (by reducing axonal loss, microglia activation, and motor paralysis) [39–41], and amyotrophic lateral sclerosis (by slowing motoneuron degeneration and gliosis) [42–44]. Finally, CB_2 targeting has even a therapeutic potential for the treatment of neuropathic pain. For instance, its activation has been recently found to efficaciously attenuate nociceptive transmission from primary afferent nerves to the spinal cord [45], thereby making CB_2 an attractive therapeutic target for the management of pain of various types and origins. Its broad pharmacological spectrum has thus prompted the design of several CB_2 selective agonists. For instance, the structure of the endogenous ligand tetrahydrocannabinol was used as starting point for the design of HU-308[46], JWH-133[47] and JBT-101[48]. Agonists with indole-based scaffold such as JWH-015[49] and AM-1241[42] were also conceived. Furthermore, a novel chemotype based on 1-(4-(pyridin-2-yl)benzyl)imidazolidine-2,4-dione core[50] was successful for the discovery of selective CB_2 agonists such as LEI-101[51] and the recently published LEI-102 [52]. Nonetheless, a small number of selective CB2 agonists such as S-777496[53] and JBT-101[48] reached the phase II human trials[43], but none of them has been yet approved for therapeutic purposes. The chemical structures of the above-mentioned compounds are reported in Figure 1.

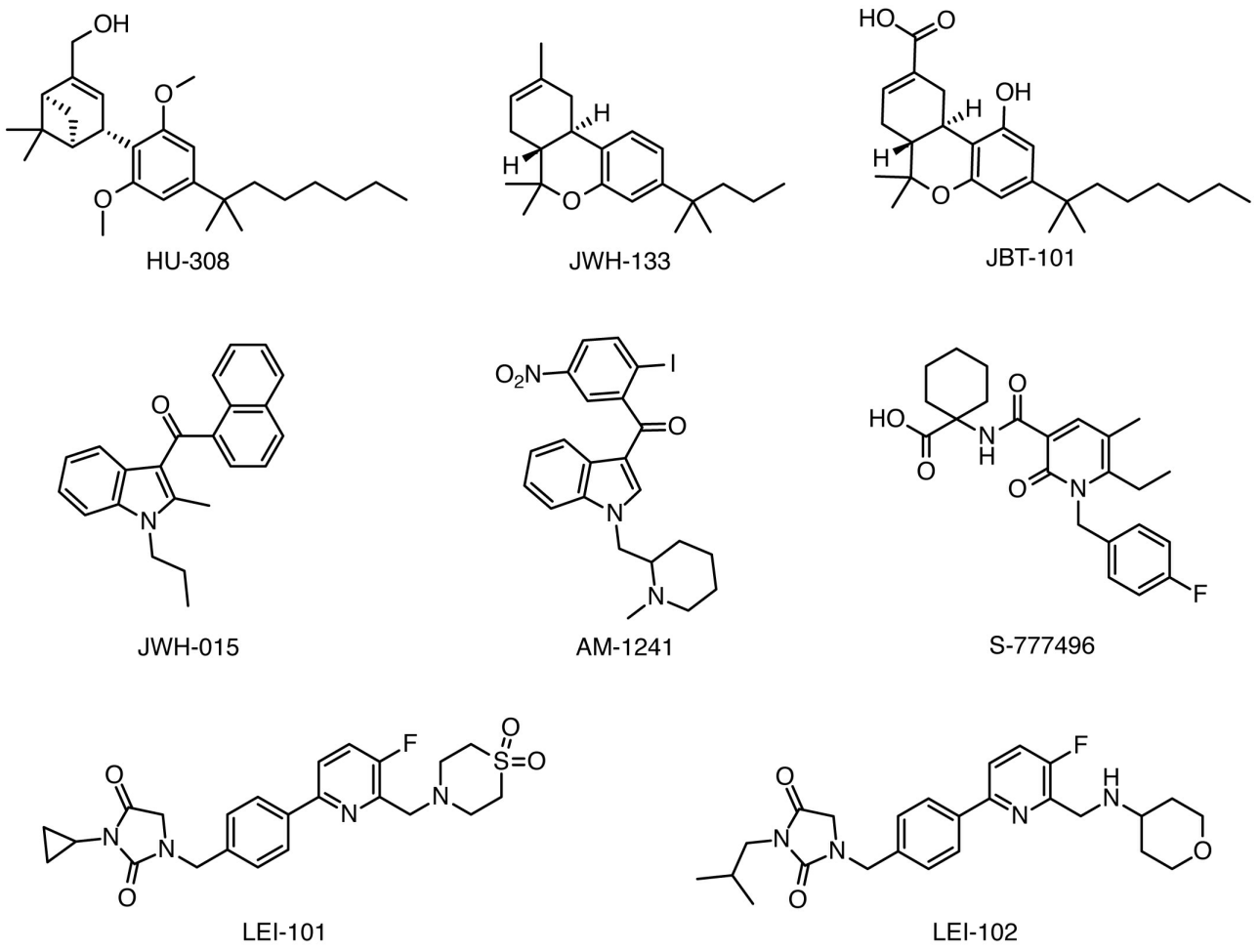

Figure 1. Chemical structures of CB_2 selective agonists.

In the present study, we developed a drug design platform by integrating modeling studies, synthesis and biochemical characterization, to identify novel selective CB_2 agonists. Starting from previous research work developed by C4T (Colosseum Combinatorial Chemistry Centre for Technology) within a medicinal chemistry program focused on novel CB modulators, our attention was mostly engaged by the benzoxazine core, an interesting privileged scaffold provided with a wide spectrum of desirable biological responses including anti-inflammatory, anti-bacterial, anti-fungal, anti-tuberculosis, anti-oxidant and anti-cancer activities [54]. Structurally, the benzoxazine is a double-ring system containing a benzene fused with a six-member heterocycle incorporating one oxygen and one nitrogen atom, whose positions can result in three different constitutional isomers, namely 1,3-, 3,1-, and 1-4-benzoxazines. Here, we focused our efforts on the 1,3-benzoxazine nucleus, a versatile structure with multiple modification sites suitable for the synthesis of a

medium-size focused library.[55,56] In particular, in light of its synthetic accessibility and its presence in several biologically active compounds,[57] we started our campaign from the 2,3-dihydro-4H-benzo[e][1,3]oxazin-4-one scaffold. Thus, we designed and synthesized a panel of 25 compounds [58] that were tested in competitive binding and functional assays toward human CB_1 and CB_2. Satisfactorily, many of these compounds displayed not only potent CB_2 agonist properties, with EC_{50} in the mid-nanomolar to low-micromolar range (110 nM - 3 μM), but also selectivity against CB_1. The most potent compound **7b5** was *in vitro* assessed for its anti-proliferative and anti-inflammatory activities. Finally, molecular dynamics (MD) studies allowed rationalizing, at an atomic level, the selective agonism of **7b5** towards CB_2, paving the way to the rational design of novel potent and specific modulators of this receptor.

RESULTS AND DISCUSSION

Design

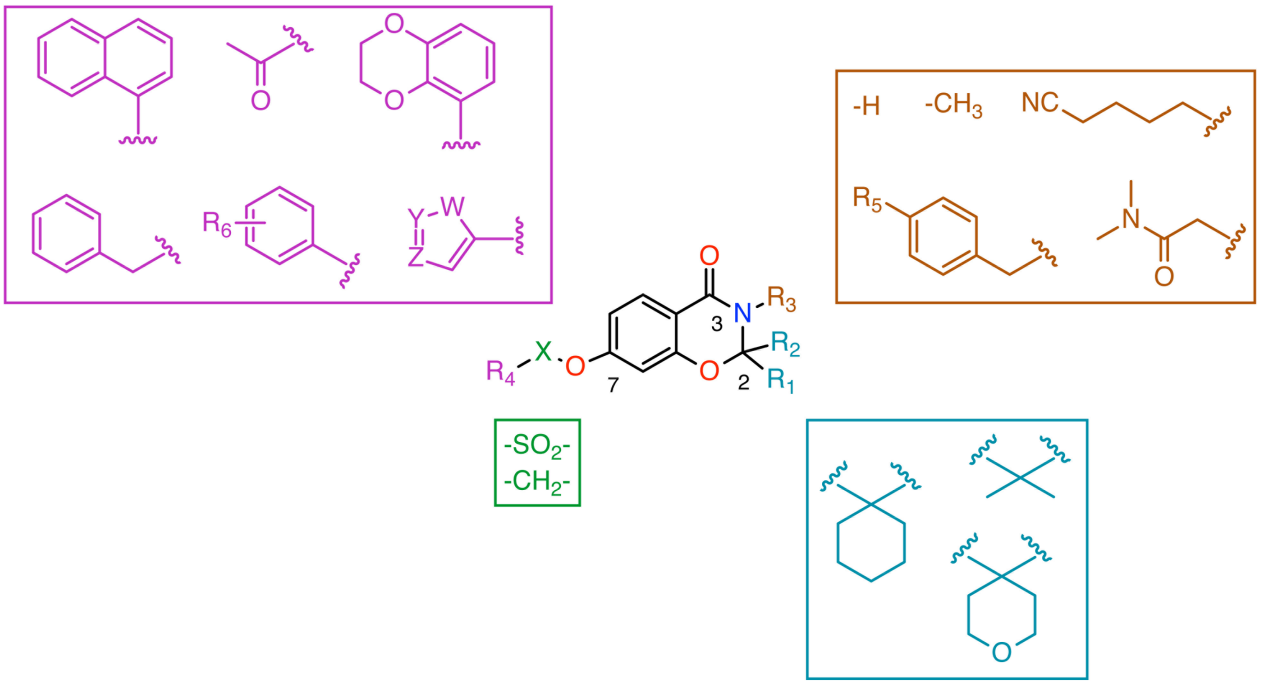

Figure 2. Schematic representation of the designed 2,3-dihydro-4H-benzo[e][1,3]oxazin-4-one derivatives. Color code: green for the X linker, cyan for the R_1 and R_2 substituents, brown and violet for the R_3 and R_4 groups, respectively.

To the best of our knowledge, compounds featuring the 2,3-dihydro-4H-benzo[e][1,3]oxazin-4-one scaffold (Figure 2) have never been explicitly related to cannabinoid effects. This was even proven by a screening of the ChEMBL (release 31, update on 12/07/2022) [59], which returned 360 compounds with molecular weight and logP ranging from 203.24 to 640.58 and from -0.02 to 5.97 (as shown in Figure S1 and Figure S2 of Supporting Information), respectively. Altogether, these compounds were experimentally related to 115 biological targets, irrespective of the species, not including the cannabinoid receptors (as reported in File_S1.csv enclosed as Supporting Information). Here, with the aim of obtaining potential CB_2 agonists we decorated the 2,3-dihydro-4H-benzo[e][1,3]oxazin-4-one scaffold with a variety of substituents at positions 2, 3 and 7 (Figure 2). More specifically, inspired by previous knowledge in the field[42,46,47,49,51,52], we introduced functional moieties able to modulate the geometrical and lipophilic properties of the resulting compounds.[2,60] Obviously, the design strategy was also driven by practical considerations such as feasibility, patentability, commercial availability and economic efforts. In this perspective: i) spiro-cyclic motifs (cyclohexyl or tetrahydropyranyl) or methyl groups were introduced at the 2 position; ii) the nitrogen at the 3 position was functionalized either with a methyl or with variously decorated benzyl groups; iii) and finally the position 7 was substituted either with oxymethylene or with oxysulfonyl bridges joined to alkyl, aromatic, or heteroaromatic substituents. Accordingly, a small library of 25 derivatives was synthesized and biologically evaluated.

Chemistry

The synthesis of our novel 2,3-dihydro-4H-benzo[e][1,3]oxazin-4-one derivatives was accomplished as depicted in Schemes 1-2. The target compounds were obtained from three main scaffolds (**4a-c**) synthesized from the 2,4-dihydroxybenzoic acid (**1**) in three steps by a common strategy,[61] as shown in Scheme 1. The carboxylic acid was converted into the corresponding primary amide (**3**) after esterification in methanol under acid catalysis and treatment of the ester (**2**)

with aqueous ammonia solution under microwave irradiation. Although the aqueous solution led to the formation of a mixture of target amide and carboxylic acid, the desired intermediate was conveniently isolated in good yields by a simple work up and the acid recovered separately. Cyclization was performed under acid catalysis using the suitable ketone as solvent for each reaction. For cyclohexanone and acetone, the corresponding methylketals were added to promote the reaction.

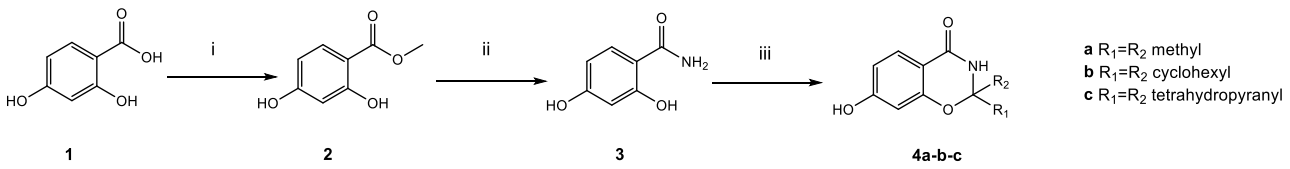

Scheme 1. Synthesis of the three different di-substituted 1,3-benzoxazin-4-one scaffolds. Reagents and conditions:

i) a. $MeOH_{dry}$, 0°C, $SOCl_2$; b. Reflux, 4h;
ii) NH_3 aq. 33%, MW (250W), 1-2h;
iii) R1/R2 ketone or acetal as solvent, NMP, 60°C;

The different di-substituted scaffolds (**4a**, R_1=R_2= methyl; **4b**, R_1=R_2= cyclohexyl; **4c**, R_1=R_2= 4-tetrahydropyranyl) were then converted into the final compounds by applying two main synthetic approaches, based on the different order of introduction of R_3 and R_4 substituents (Scheme 2).

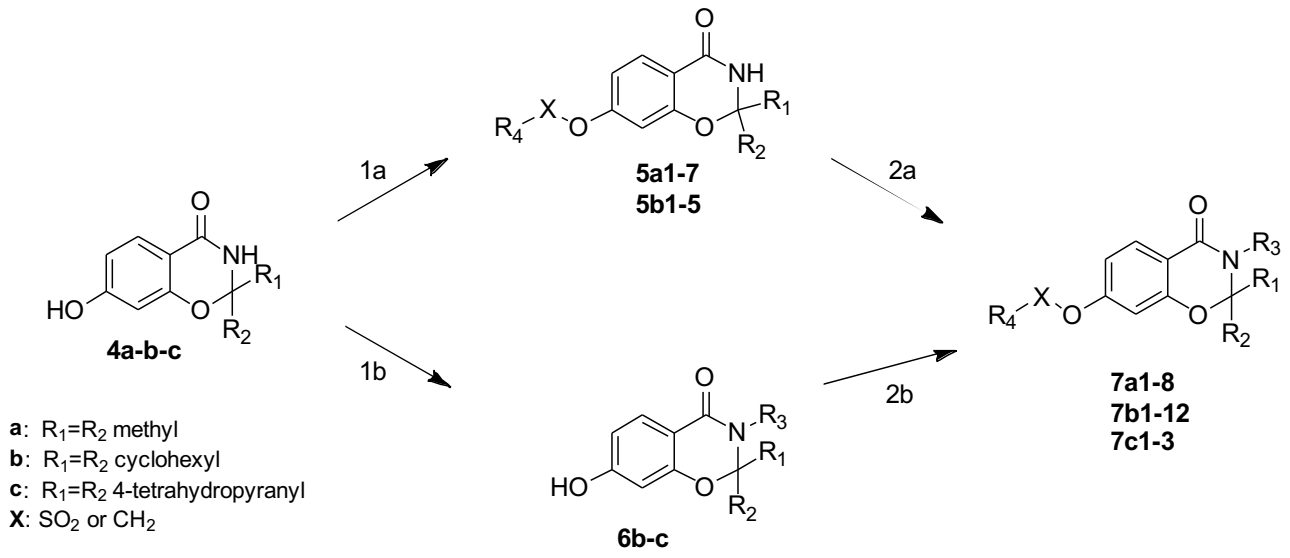

160
161

162 **Scheme 2.** Overall synthetic strategy for the synthesis of the 25 2,3-dihydro-4H-
163 benzo[e][1,3]oxazin-4-one derivatives.

164 Reagents and conditions:

165 1a) DMF, K_2CO_3 3 eq, R4-XCl 2 eq, on rt;
166 2a) NaH 2.2 eq, DMF; R3Br 1.5 eq10hs rt;
167 1b) i) MOMCl 2eq, K_2CO_3 3 eq, DMF, 10h, rt; ii) NaH 2.2 eq, DMF; BzBr 1.5 eq10hs rt iii) 6N HCl/MeOH, rt, on;
168 2b) DMF, K_2CO_3 3 eq, R4-SO_2Cl 2eq, on rt.

169

170 The approach a) was applied for those derivatives of scaffolds **4a** and **4b** that displayed a high
171 variability on both R_3 and R_4 substituents. In this strategy, ethers and sulfonic esters (**5a**-**b**) were
172 obtained by adding the different alkyl bromides or sulfonyl chlorides, respectively, to scaffolds **4a-**
173 **b**, in DMF with potassium carbonate. Structural description of the synthesized intermediates is
174 detailed in Table S1 of the Supporting Information. Most compounds were used as crudes in the
175 subsequent reaction, except for two of the synthesized intermediates that were purified and enclosed
176 in the set of final compounds for *in vitro* screening (**5a2**, **5b1** in Table 1). The *N*-alkylation of the
177 obtained ethers and sulfonic esters was performed using sodium hydride and the different
178 commercially available alkyl halides, providing derivatives **7a1-8** and **7b1-5** detailed in Table S3
179 section A of the Supporting Information.

A set of compounds sharing the R_3 benzylamine substituent and the sulfonyl moiety at the position X (Figure 2) were synthesized according to the approach b), either for scaffold **4b** or **4bc**. In this case, the 7-hydroxy group was protected with methoxymethyl ether (MOM) for the selective N-alkylation, introducing the R_3 benzyl group, then deprotection of MOM afforded intermediates **6b-c** that were reacted with target sulfonyl chlorides to provide the desired R_4 substitution (derivatives **7b5-12** and **7c1-3** in Table S3 section B of the Supporting Information).

Compound **7b5** was synthesized according to both strategies to compare yields and overall feasibility, also in the view of future scale up. A detailed structural description of the 25 derivatives is shown in Table S3 of the Supporting Information.

Table 1. CB_2 and CB_1 pEC_{50} experimental values of 2,3-dihydro-4H-benzo[e][1,3]oxazin-4-one derivatives obtained from [^{35}S]GTPγS binding assay

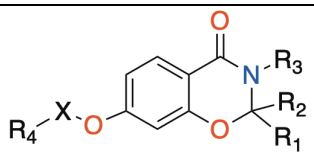

ID	R_1	R_2	R_3	R_4	X	pEC_{50} CB_2[a]	pEC_{50} CB_1[a]
5a2	CH_3	CH_3	H	1-naphthyl	SO_2	-	-
5b1	cyclohexyl		H	2'-NO_2-C_6H_4	SO_2	5.67 ± 0.32	< 5*
7a1	CH_3	CH_3	4'-F-C_6H_4-CH_2	4'-OCF_3-C_6H_4	CH_2	-	-
7a2	CH_3	CH_3	CH_3	1-naphthyl	SO_2	5.53 ± 0.25	5.14 ± 0.28
7a3	CH_3	CH_3	4'-F-C_6H_4 -CH_2	4'-CH_3-C_6H_4	SO_2	6.71 ± 0.29	< 5 *
7a4	CH_3	CH_3	C_6H_5-CH_2	$(CH_3)_3$ C(O)	CH_2	-	-
7a5	CH_3	CH_3	CH_3	4'-(C_6H_4-O)-C_6H_4	SO_2	-	-
7a6	CH_3	CH_3	N$(CH_3)_2$C(O)CH_2	4'-Br-C_6H_4	SO_2	-	-
7a7	CH_3	CH_3	4'-$(CH_3)_2$CH-C_6H_4-CH_2	3'-OCH_3-C_6H_4	CH_2	-	-
7a8	CH_3	CH_3	4'-F-C_6H_4-CH_2	3'-OCH_3-C_6H_4	CH_2	-	-
7b1	cyclohexyl		4'-$(CH_3)_2$CH-C_6H_4-CH_2	3'-OCH_3-C_6H_4	SO_2	-	-
7b2	cyclohexyl		CN-$(CH_2)_4$	3'-OCH_3-C_6H_4	SO_2	6.11 ± 0.19	< 5*
7b3	cyclohexyl		4'-CN-C_6H_4-CH_2	3-(1-CH_3-1H-pyrazolyl)	SO_2	6.43 ± 0.12	< 5*

7b4	cyclohexyl	4'-CN-C_6H_4-CH_2	4'-OCF_3-C_6H_4	CH_2	-	-
7b5	cyclohexyl	C_6H_5-CH_2	2-thienyl	SO_2	6.97 ± 0.20	< 5
7b6	cyclohexyl	C_6H_5-CH_2	4'-(4-Cl-C_6H_4)-C_6H_4	SO_2	-	-
7b7	cyclohexyl	C_6H_5-CH_2	3'-CN-C_6H_4	SO_2	6.45 ± 0.18	< 5
7b8	cyclohexyl	C_6H_5-CH_2	4'-OCH_3-C_6H_4	SO_2	5.83 ± 0.16	< 5
7b9	cyclohexyl	C_6H_5-CH_2	4'-CN-C_6H_4	SO_2	6.54 ± 0.12	< 5
7b10	cyclohexyl	C_6H_5-CH_2	4-(1-CH_3-1H-imidazolyl)	SO_2	6.00 ± 0.15	< 5
7b11	cyclohexyl	C_6H_5-CH_2	C_6H_5-CH_2	SO_2	6.12 ± 0.10	< 5
7b12	cyclohexyl	C_6H_5-CH_2	3'-OCH_3-C_6H_4	SO_2	6.38 ± 0.09	< 5
7c1	4-tetrahydro-pyranyl	C_6H_5-CH_2	3'-NO_2-C_6H_4	SO_2	6.69 ± 0.17	< 5
7c2	4-tetrahydro-pyranyl	C_6H_5-CH_2	6-(1,4-benzodioxan)	SO_2	-	-
7c3	4-tetrahydro-pyranyl	C_6H_5-CH_2	4'-NO_2-C_6H_4	SO_2	-	-
1 μM **JWH-015** (reference CB2 agonist)					233 ± 14[b]	-
1 μM **ACEA** (reference CB1 agonist)						241 ± 18[b]

[a] Mean ± SEM of 3 independent experiments performed in quintuplicate; [b] percentage of stimulation; *indicates inverse agonist at CB_1.

Biological Studies

We first evaluated the binding affinity of all the newly synthetized compounds towards CB_2, based on a high-throughput screening radioligand binding assay standardized in our laboratories.[62] To this aim, commercially available membranes overexpressing human CB_2 were used for assessing the ability of each compound (at 0.1 μM) to compete with [^{3}H]CP55,940 for binding to CB_2. In this assay, all the compounds displayed a residual activity below the cutoff (≤ 80%). After that, all the molecules were tested in the [^{35}S]GTPγS binding assay at 10 and 100 μM concentrations, to establish their activity profile as agonist, antagonist or inverse agonist. This approach allowed identifying 13 agonists. By the same assay, these agonists were analysed, at increasing (0 - 100 μM) concentrations, for their efficacy at CB_2; the molecules displayed EC_{50} values ranging from 110 nM to 3 μM (i.e., 5.53 ≤pEC_{50}≤ 6.97) as shown in Table 1. Binding selectivity for CB_2 over CB_1 was assessed only for molecules showing a clear agonistic behaviour. Among these agonists, **7b5** turned out to be the most potent compound, showing a EC_{50} value of 110 nM (i.e., pEC_{50} = 6.97) for CB_2 (Figure S3 of Supporting Information) and a remarkable selectivity compared to CB_1 (EC_{50} > 10

μM). Therefore, we prioritized this compound to evaluate its biological activity. Since it has been previously described that pharmacological activation of CB_2 triggers antitumor responses in preclinical models of breast cancer,[63] we analysed the effect of **7b5** on breast tumour cells in terms of proliferation and clonogenic potential. As demonstrated by MTT assay, **7b5** significantly impaired the proliferating capacity of triple-negative breast cancer BT549 cells (Figure 3a). The inhibitory effect was already evident after 24 h incubation with 1 and 10 μM of **7b5**, and after 72 h at all tested concentrations, and was dose-dependent (Figure 3a). Of interest, the same effect was produced in two additional breast cancer cell lines, the triple negative MDA-MB-231 and HER2-positive HCC1954 breast cancer cells, while the viability of normal epithelial MCF-10A breast cells remained unaltered (Figure S4 of the Supporting Information), thus suggesting that **7b5** selectively targets cancer cells without affecting normal cells. Based on these results, we chose to use 10 μM **7b5** for the subsequent experiments. **7b5** also strongly and significantly inhibited the capacity of breast cancer cells to survive and undergo unlimited division. Indeed, as assessed by colony forming unit (CFU) assay, BT549 cells grown in the presence of **7b5** displayed a decreased number of colonies (75.4% reduction) with respect to vehicle-treated cells (Figure 3b).

Superimposable data were obtained when we evaluated BT549 cell response to the CB_2 reference agonist JWH-015. Indeed, as assessed by CFU experiments, this selective CB_2 agonist, used at 0.1 μM produced an almost identical decrease in cell proliferation (Figure S5 of the Supporting Information) and colony formation capacity observed with **7b5** (Figure 3b). The selected concentration of JWH-015 was chosen on the basis of its Ki values for CB_2 and CB_1 (13.8 and 383 nM, respectively)[64] and our MTT results (Figure S5 of the Supporting Information). Collectively, these data indirectly suggested that both **7b5** and JWH-015 may act through the same receptor. To get a more direct and solid proof of our hypothesis and, simultaneously, to rule out the involvement of CB_1 and other related receptors, especially those previously associated with breast cancer, such as GPR18 and GPR55[65–67] , we finally performed MTT assays in BT549 cells transiently

transfected with a commercially available siRNA targeting *CNR2* (the CB_2 encoding gene) or with a scramble oligo (Figure S6 of the Supporting Information and Figure 3c). *CNR2* silencing completely prevented the inhibitory action of both **7b5** and JWH-015 (Figure 3c), thus confirming the involvement of CB_2 in the anti-cancer effects of the newly synthesized compound. As additional readout to evaluate the potential of our selected 1,3-benzoxazine derivative, we tested its anti-inflammatory potential, by measuring release of interleukin-6 (IL-6) and tumor necrosis factor (TNF)-α from BT549 cells. Indeed, it is well established that chronic inflammation within the tumor microenvironment correlates with increased invasiveness and poor prognosis of several malignancies, including breast cancer. [68] Moreover, such a pro-inflammatory milieu is further potentiated by cancer cells able to release a huge amount of pro-inflammatory mediators, such as IL-6 and TNF-α.[69–71] As shown in Figure 3d, 48-hour incubation with 10 μM **7b5** drastically attenuated IL-6 and TNF-α secretion: in fact, the medium derived from **7b5** treated cells contained approximately less than 50% and 70% of TNF-α and IL-6, respectively, with respect to medium from vehicle-treated cells. The anti-inflammatory activity depended on CB_2, as **7b5** effect was significantly reversed by *CNR2* siRNA (Figure 3d). Inflammation and cancer share common molecular routes, among which extracellular signal-regulated kinase (ERK) 1/2 cascade represents one of the most important oncogenic drivers of human cancer.[72] As this signalling is also counted among alternative CB_2 coupled effector pathways,[2,73] we tested whether **7b5** dependent activation of CB_2 might control ERK 1/2 activity. As shown in Figure 3e, **7b5** downregulated ERK 1/2 phosphorylation in a biphasic time-dependent fashion: amounts of phosphorylated ERK slowed down to about 30% of vehicle-treated cells within five minutes, and then returned to nearly basal levels in the next five minutes to drastically decrease thereafter. Such an effect was completely abrogated by CB_2 knockdown, that significantly (even though slightly) upregulated ERK 1/2 phosphorylation.

Further studies are necessary to fully elucidate the exact molecular mechanism underlying **7b5**/CB_2-mediated anti-oncogenic and anti-inflammatory effects; CB_2, indeed, may exert anti-tumor activity through multiple mechanisms of actions, also depending on the biased CB_2 agonism. [2,26,74–78] Nonetheless, whatever the detailed mechanism and functional selectivity of this candidate agonist, our preliminary results point out that **7b5** might represent an alluring lead compound for the design of novel CB_2 agonists to be exploited as valuable drugs against cancer and, more generally, inflammation-related diseases.

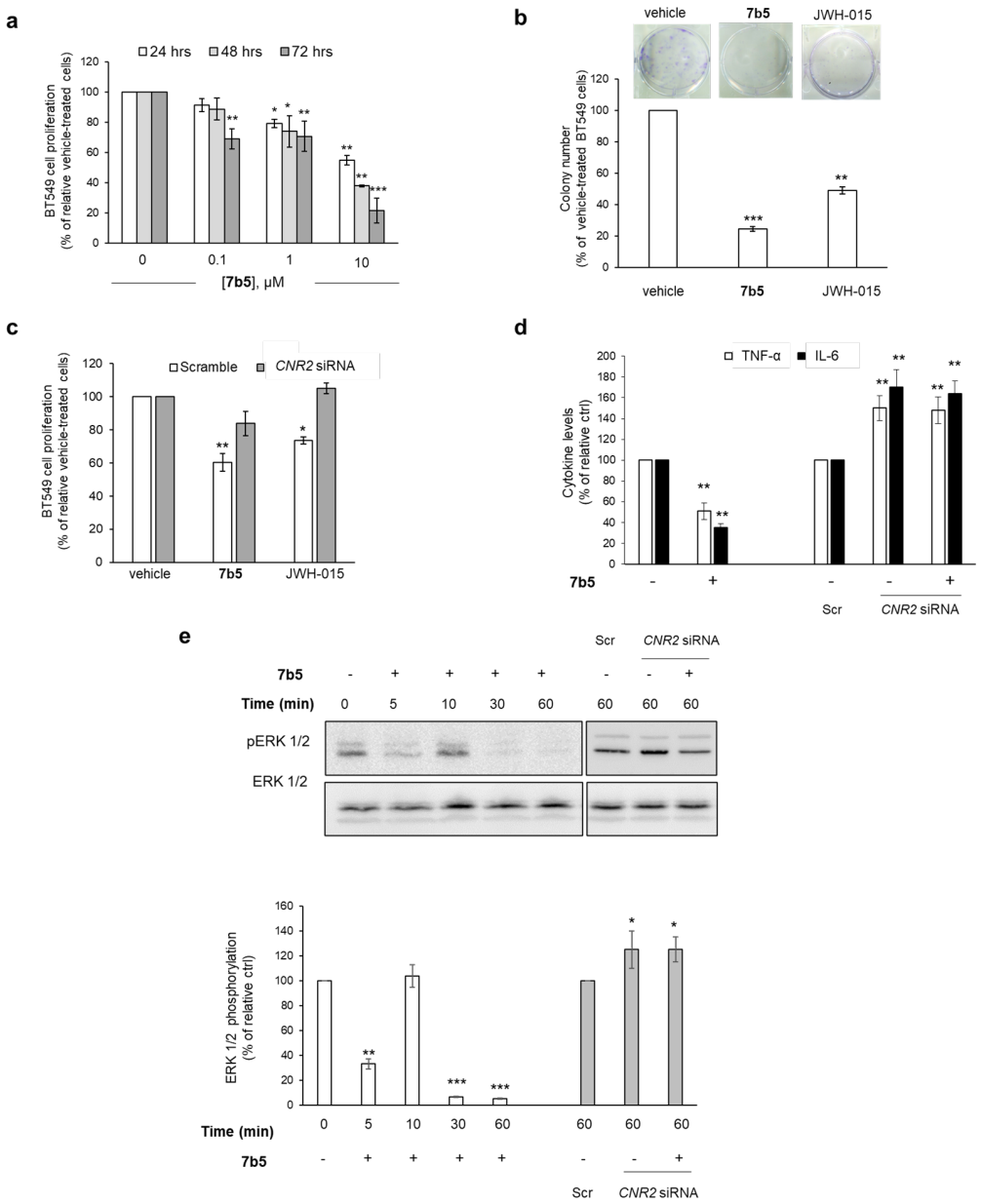

Figure 3. Anti-proliferative and anti-inflammatory effects of 7b5 on BT549 breast cancer cells. a) MTT assay performed on BT549 cells treated with either vehicle (0) or **7b5** at indicated concentrations, for 24, 48 and 72 hours. Values are reported as percentage of relative vehicle, arbitrarily set to 100%. Data represent the mean ± SEM of three experiments, each repeated at least in quintuplicate. *p < 0.05, ** p < 0.01 and *** p < 0.001 *vs* vehicle. b) Colony forming unit (CFU) assay performed with BT549 cells grown for at least 14 days, in the presence of either vehicle or 10 µM **7b5** or 0.1 µM JWH-015. Photographs are representative of three independent experiments, each repeated at least in triplicate. Histogram shows the colony number reported as percentage of

vehicle-treated cells, arbitrarily set to 100% (absolute colony number = 123.67 ± 5.32). Data are shown as mean ± SEM. *** $p < 0.001$ *vs* vehicle. c) MTT assay performed on BT549 cells transiently transfected with either scramble oligo (Scr) or *CNR2* siRNA and treated with either vehicle or 10 μM **7b5** or 0.1 μM JWH0-15, for 24 hours. d) Measurement of TNF-α and IL-6 levels in medium from BT549 cells left untransfected or transfected with either scramble oligo (Scr) or *CNR2* siRNA and treated with either vehicle (-) or 10 μM **7b5** for 48 hours incubation. Cytokines content was evaluated by the means of ELISA assay. Results are expressed as percentage of vehicle-treated cells set to 100% (absolute value for TNF-α and IL-6 levels: 6.5 ± 0.2 pg/mL culture medium and 6413.3 ± 235.6 pg/mL culture medium, respectively). Values are the means ± SEM of three independent experiments, each performed in triplicate. ** $p < 0.01$ *vs* relative vehicle-treated cells. e) Dose-response curve of ERK 1/2 phosphorylation in BT549 cells left untransfected or transfected with either scramble oligo (Scr) or *CNR2* siRNA and incubated at 37°C, in the absence (-) or in the presence of 10 μM **7b5**, for the indicated periods of time. Phosphorylated ERK 1-2 (p-ERK 1-2) and ERK 1-2 were detected by Western blot analysis. Blots are representative of three independent experiments. Histograms (lower panel) show the densitometric analysis of p-ERK 1-2 expression levels normalized to the levels of ERK 1/2 and reported as percentage of relative control arbitrarily set to 100 %. * $p < 0.05$ and ** $p < 0.001$ *vs* relative vehicle-treated cells.

Structure Activity Relationships

The activity data reported in Table 1 disclose preliminary but intriguing structure activity relationships, which can be very helpful to elucidate the molecular bases of the CB_2 potency, efficacy and selectivity of our newly synthesized derivatives. First of all, the presence of the sulfonyl group at the X position seems crucial to afford effective CB_2 agonists: in fact, its replacement with a methylene linker affords inactive compounds (**7a1**, **7a4, 7a7**, **7a8**, and **7b4**). This is presumably due to the peculiar spatial properties of the sulfonyl group (i.e. tetrahedral

298 geometry), which may allow the ligand to assume a conformation competent for binding to the
299 receptor. The introduction of either two methyl groups or a spirocyclic system (spiro-cyclohexyl or
300 4-tetrahydro-pyranyl ring) at positions R_1 and R_2 is well tolerated; in particular, the presence of a
301 spiro-cyclohexyl ring (compounds **7b1-12**) seems to be particularly favorable, likely due to an
302 overall increase in lipophilicity. Similarly, the functionalization of the nitrogen at the position 3 on
303 the 1,3-benzoxazine ring with a benzyl group (**7b5-12**) is desirable to obtain derivatives with good
304 CB_2 potency and selectivity. The size of the substituents at the R_4 position is very relevant for
305 tuning the activity: generally, aromatic five-member rings are preferred to enhance binding and
306 selectivity (**7b5, 7b10**); however, *para*-substituted phenyl ring with a small group, such as methyl
307 (**7a3**), or even better with a small and electron withdrawing group, such as cyano (**7b9**), can be
308 important for tuning CB_2 selectivity. On the other hand, the activity and, to a lesser extent,
309 selectivity of *meta*-substituted phenyl ring depends on the size of the substituents, with the
310 following activity trend: CN (**7b7**) > NO_2 (**7c1**) > OCH_3 (**7b12**). Finally, the insertion of bulkier
311 (**7a2**) or even worse, longer substituents (**7b6**) is detrimental for both affinity and selectivity.

312

313 **Computational Studies**

314 To elucidate the binding mode of our newly developed CB_2 agonists, we performed extensive
315 molecular modeling studies on **7b5**, the most promising ligand of the series.

316

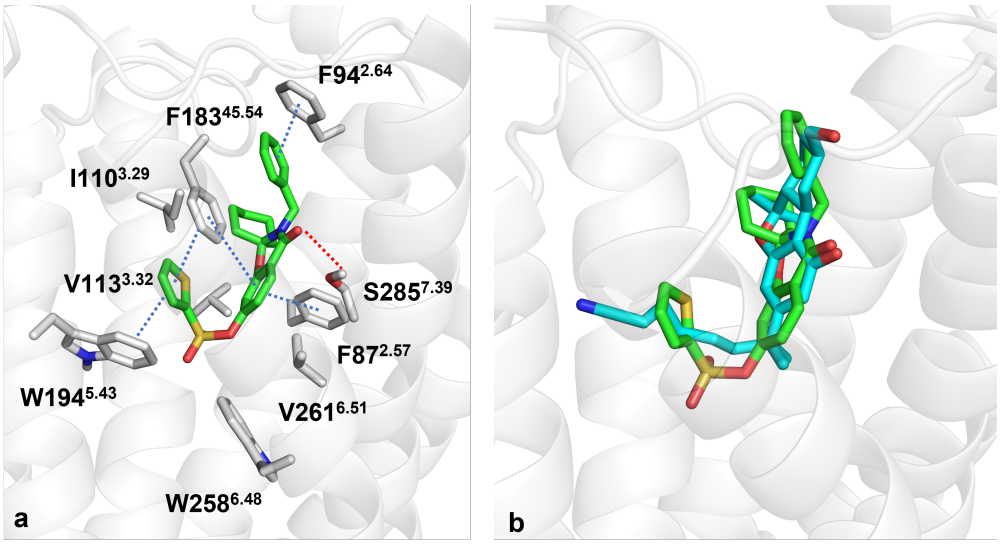

Figure 4. a) Top scored docking pose of **7b5** at the CB_2 binding pocket. The receptor is shown as grey cartoons, whereas the binding site residues are highlighted as sticks. The ligand is depicted as green sticks. Blue and red dotted lines indicate π-π contacts and hydrogen bonds, respectively. b) Superimposition of the top scored docking pose of **7b5** with the cognate crystal CB_2 agonist structure (cyan sticks).

First, molecular docking simulations of this compound were carried out with Glide in the Extra Precision (XP) mode (please see Experimental section for details)[79] in the recently solved crystal structure of the agonist-bound form of CB_2 (PDB ID: 6KPC).[80] In the top scored docking pose (Figure 4a), **7b5** binds in a bent conformation at the CB_2 orthosteric site, where it can form a dense network of aromatic interactions. In detail: i) the 1,3-benzoxazine core is sandwiched between $F87^{2.57}$ and $F183^{45.54}$; ii) the thienyl moiety is trapped between the side-chains of $F183^{45.54}$ and $W194^{5.43}$; and iii) the benzyl group can establish a π-π interaction with $F94^{2.64}$. Additional hydrophobic contacts are then established by the cyclohexyl and 1,3-benzoxazine moieties with the side-chains of $I110^{3.29}$ and $V113^{3.32}$, and of $V261^{6.51}$, respectively, which can further stabilize the binding mode. Besides these lipophilic interactions, the carbonyl group of **7b5** can form a H-bond with $S285^{7.39}$, which has been reported as important for the binding of CB_2 agonists.[52,80] On the other hand, in line with its agonist profile, **7b5** is unable to engage the toggle switch residue

W258$^{6.48}$, which is in fact generally involved in direct interactions with CB_2 antagonists. Indeed, these are usually endowed with bulky aromatic groups able to form T-shape interactions with the indole ring of the tryptophan residue[81]. Notably, as shown in Figure 4b, the top scored docking pose of **7b5** is well superimposed with the cognate crystal CB_2 agonist structure, which confirms the robustness of our docking results. Interestingly, a comparable binding mode and interaction scheme involving hydrophobic residues such as F87$^{2.57}$, F94$^{2.64}$, I110$^{3.29}$, V113$^{3.32}$, and W194$^{5.43}$ were also depicted for well-known CB_2 selective agonists like HU-308 in a recently released CB_2 cryo-EM structure. [52]

Nevertheless, to further evaluate the reliability and the energetics of the docking pose by including full receptor flexibility and solvent effects, we carried out 3 μs MD simulations on the **7b5**-CB_2 complex in explicit water and membrane by using GROMACS (please see Experimental section for details).[82] During the first steps of the simulation the ligand slightly rearranges to assume a conformation (Figure 5a) that is then maintained throughout the trajectory. This can be appreciated by looking at the ligand heavy atoms RMSD plot that is shown in Figure 5b. To get more insights into such small changes, we evaluated the stability over time of the **7b5** and receptor contacts depicted from docking analysis (as shown in Figure S7 of the Supporting Information). First, we monitored the distances between the centroids of the aromatic rings involved in the aforementioned π-π contacts, observing that the interaction with F94$^{2.64}$ by the benzyl ring of **7b5** is tightened over time (Figure 5c). Then, we evaluated the distance between the ligand carbonyl group and the S285$^{7.39}$ side-chain, noticing that the H-bond between these two moieties is weakened throughout the simulation. This would suggest that, in future rounds of chemical optimization, structural modification could be introduced at this position of **7b5** to further improve the ligand binding potency.

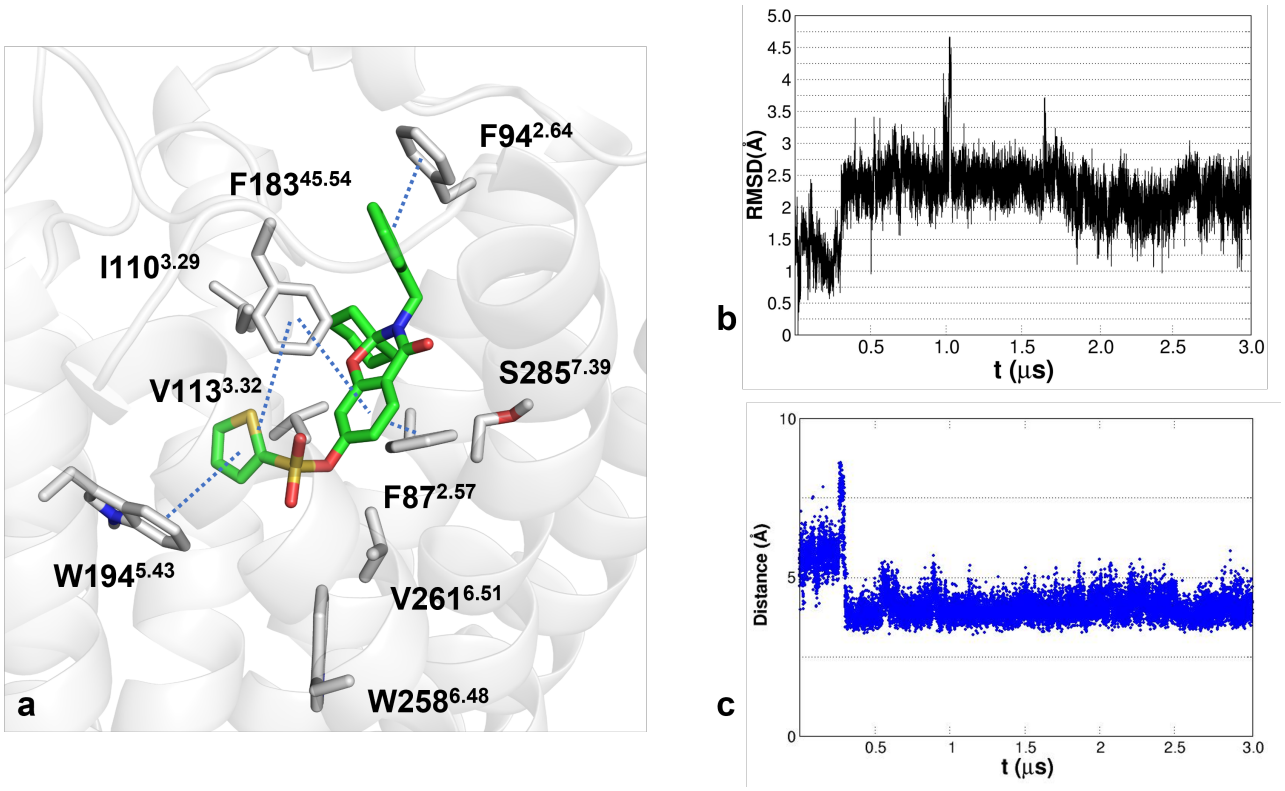

359

360 **Figure 5.** a) MD posing of **7b5** at the CB_2 orthosteric site. The receptor is shown as grey cartoons,
361 whereas binding site residues are highlighted as sticks. The ligand is depicted as green sticks. π-π
362 interactions are shown as dashed blue lines. b) RMSD plot of ligand heavy atoms throughout the
363 trajectory. Prior to calculations, trajectory frames were aligned on the C_α of all the helices. c) Plot
364 of the distance between the centroids of the F94$^{2.64}$ phenyl group and **7b5** benzyl ring along the MD
365 simulations.

366

367 In order to analyze, at molecular level, the agonist behavior of **7b5**, we then monitored throughout
368 the trajectory some of the receptor structural features that have been reported elsewhere as
369 hallmarks of its activated state.[80] First, as shown in Figure 6, we evaluated the χ^2 torsional angle of
370 the toggle switch W258$^{6.48}$, showing that this residue remains in the 'agonist state' (see Figure 6b)
371 for the whole simulation. This is probably due, as reported above, to the absence of direct
372 hydrophobic contacts with **7b5**, at variance with what has been described elsewhere for receptor-
373 antagonist complexes [83]. Moreover, we observed that the "ionic lock" between R131$^{3.50}$ and

D240$^{6.30}$, which normally holds the receptor in the inactive state, is not formed at any time during the simulation (Figure S8 of the Supporting Information).

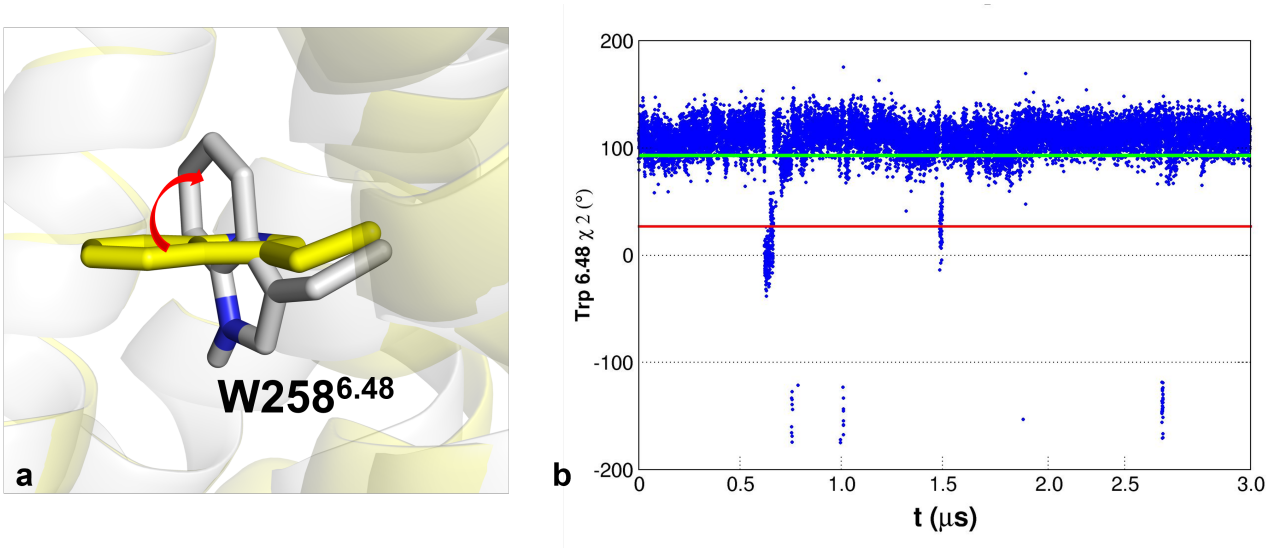

Figure 6. a) Zoomed in view of the agonist and antagonist states of toggle switch W258$^{6.48}$, which are, respectively, colored in white and yellow. The former corresponds to the average conformation assumed by the residue along the MD simulation, while the latter is taken from the antagonist-bound X-ray CB_2 structure (PDB ID: 5ZTY) [17]. b) Plot (as blue dots) of the W258$^{6.48}$ χ^2 torsional angle throughout the simulation. Reference values for agonist (green line) and antagonist (red line) states were taken from [81,83], and are shown as green and red lines, respectively.

Interestingly, the interaction model of **7b5** with CB2 is in agreement with the observations derived from SAR studies. Firstly, our simulations showed that the sulfonyl group is effective in inducing the proper ligand binding geometry, although it is unable to experience specific interactions with CB_2 residues. Secondly, MD studies indicated that the 2-thienyl moiety of **7b5** engaged a narrow aromatic pocket whose room could potentially accommodate only similarly sized aromatic rings such as mono-substituted phenyl (e.g. **7a3**, **7b12** and **7c1**), pyrazolyl or imidazolyl rings (e.g. **7b3** and **7b10**); accordingly, the introduction of bulkier moieties such as a biphenyl (**7b6**) and 1,4-benzodioxan (**7c2**) is detrimental for receptor binding and/or activation. Likewise the thienyl

moiety, the ligand benzyl group is predicted to bind to a restricted hydrophobic cleft establishing contacts with residues such as F94$^{2.64}$, which are important for receptor binding and activation. Indeed, compounds either devoid of this substituent (e.g. **5a2** and **7a6**) or endowed with more extensive moieties (**7b1**) generally show a drop in the binding affinity. For the sake of comparison, **7a3** and **7b9** were docked on the relaxed post-MD structure of the CB_2 receptor. As shown in Figure S9 of the Supporting Information, **7a3** and **7b9** disclosed the same posing experienced by the most active **7b5** by establishing very similar hydrophobic interactions within the CB_2 binding site through F87$^{2.57}$, F94$^{2.64}$, F183$^{45.54}$ and W194$^{5.43}$ residues.

Finally, we tried to exploit our MD calculations to speculate about the molecular basis of the selectivity of **7b5** against the CB_1. Since a correct overlay of the static CB_1 crystal structure with the ligand-bound CB_2 conformation taken from our MD simulation was not possible, we built a 'dynamic homology model' of CB_1 using the latter as a template, and then superimposed the two structures. Given the high sequence identity of the two receptors at the orthosteric site, this approach allowed us to identify possible single point substitutions supposedly responsible for bad contacts or steric clashes with **7b5** in CB_1, and would, in turn, support the lack of activity of this ligand towards this isoform. Notably, only three mutations differentiate the binding site of the two cannabinoid receptors; in fact, I110$^{3.29}$, L182$^{45.53}$ and V261$^{6.51}$ in CB_2 are, respectively, replaced by L193$^{3.29}$, I267$^{45.53}$ and L359$^{6.51}$ in CB_1 (Figure 7a). Given the isomeric nature of leucine and isoleucine residues, the I110/L193 and L182/I267 mutations are unlikely to affect the binding of **7b5** to CB_1. Conversely, as shown in Figure 7b and Figure 7c, the CB_1 L359$^{6.51}$ residue, which is bulkier than the corresponding V261$^{6.51}$ in CB_2, could clash with the oxysulfonyl bridge of **7b5**, and might thus prevent a good tethering. These observations are in agreement with recent mutagenesis data showing that the binding potency of other CB_2 selective agonists, such as HU308, is unaffected and significantly reduced in the presence of the I110$^{3.29}$L and the V261$^{6.51}$L substitutions. [52]

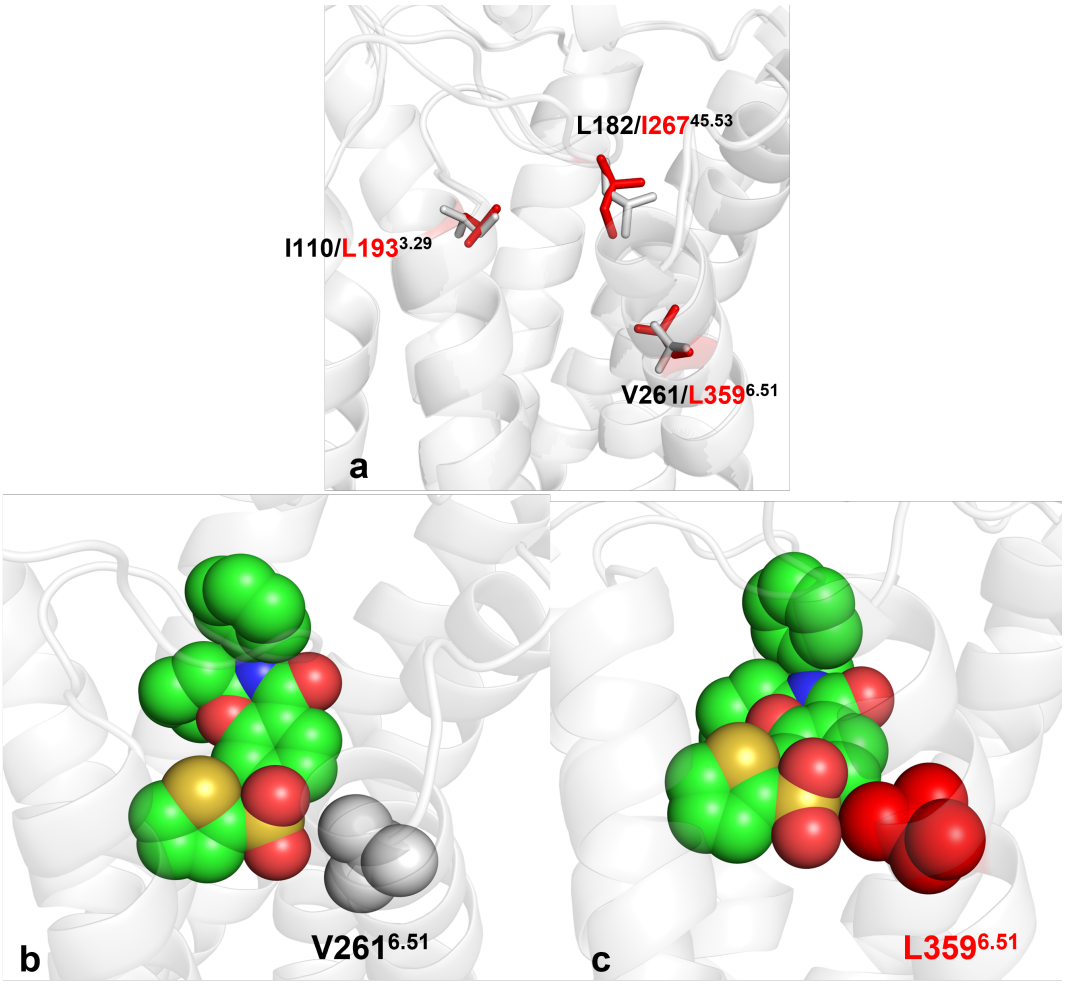

Figure 7. a) Mutated residues within the orthosteric sites of CB_1 (red sticks) and CB_2 (grey sticks) are shown in panel. Receptors are shown as grey cartoons. **7b5** at the (b) CB_2 (MD structure) and (c) CB_1 (homology model) binding pockets. Receptors are shown as grey cartoons. **7b5**, CB_2 $V261^{6.51}$ and CB_1 $L359^{6.51}$ are rendered as green, gray, and red spheres, respectively

CONCLUSION

In this investigation, we designed and synthesized a small focused library of 2,3-dihydro-4H-benzo[e][1,3]oxazin-4-one derivatives as potential CB_2 agonists. Notably, many of these compounds displayed EC_{50} values in the mid-nanomolar to low-micromolar range for human CB_2 and good selectivity over the CB_1 receptor. In particular, compound **7b5** showed an EC_{50} of 110 nM (i.e., $pEC_{50} = 6.97$) for CB_2 that was much higher for CB_1 ($EC_{50} > 10$ µM). In biological assays, this molecule demonstrated to impair in a CB_2-dependent manner the proliferation and clonogenic

potential as well as the cytokine release activity of triple negative breast cancer BT594 cells. Furthermore, **7b5** was able to reduce the activation of extracellular signal-regulated kinase (ERK) 1/2, a key pro-inflammatory and oncogenic enzyme, highlighting the anticancer versatility of **7b5**. Thus, although already employed as privileged structure in medicinal chemistry, the 1,3-benzoxazine scaffold has been here repurposed for the first time to design selective agonists of CB_2 as potential therapeutic tools against pathologies where this receptor is dysregulated, including neurological and fibrotic diseases, pain, osteoarthritis and cancer.[84] On the other hand, the high versatility and of the **7b5** nucleus will prompt the exploration of an off-patent chemical space in the search of even more potent and selective novel modulators of cannabinoid receptors. In this perspective, precious hints were provided by our MD studies, both for improving the CB_2 *versus* CB_1 selectivity based on the key role played by the V261/L359$^{6.51}$ substitution and tuning the agonist action based on the interplay with the toggle switch residue W258$^{6.48}$.

EXPERIMENTAL SECTION

General Information

Reagents and solvents were purchased from commercial sources and used without further purification. Flash chromatography was performed on E. Merck silica gel. RP purifications were performed by using a Gilson HPLC-UV system (321/H2M pumps, UV/Vis 152, Fraction collector 2020).

^{1}H NMR spectra were recorded in the specified deuterated solvents on a Bruker Avance 300 spectrometer operating at 300 MHz. Chemical shifts are reported in ppm (d) from the tetramethylsilane (TMS) resonance in the indicated solvent (TMS: d=0.0 ppm). Compound purities and mass spectra were determined by using an LC-UV-MS platform (Gilson/ThermoFinnigan and Agilent 1260 Series - Thermo Finnigan Mass Analayzer Thermo Surveyor MSQ and Agilent 6100 Series Single Quad LC/MS spectrometer) by means of the positive electrospray ionization

technique (ES+) with a mobile phase of acetonitrile/water containing 0.05% trifluoroacetic acid (TFA). In few cases negative electrospray ionization technique (ES-) with a mobile phase of acetonitrile/water containing 0.05% ammonium formate was applied.

Based on the HPLC analysis, the purities of final compounds were all ≥ 95%. ^{1}H and ^{13}C NMR spectra of final compounds for screening were recorded on a Bruker Avance 400 MHz spectrometer equipped with Cryo Platform PRODIGY probe. For a better evaluation of the structural assignment, 2D spectra analyses (^{1}H-^{13}C HSQC and HMBC) were performed for some of the final compounds.

General Procedures for Preparation of Intermediates

*Methyl 2,4-dihydroxybenzoate (**2**)*

2,4-dihydroxybenzoic acid **1** (20.0 g, 130 mmol) was dissolved in methanol (100 mL) in a 250 mL flask, held over a flame and placed under a nitrogen atmosphere. The mixture was subjected to agitation and cooled to 0 °C with an ice bath. Thionyl chloride (10.0 mL, 137 mmol) was added drop by drop. After 30 minutes, the mixture was placed under reflux (65 °C) and left under agitation for 4 hours. The mixture was dried at reduced pressure, recovered with ethyl acetate (100 mL) and washed with aqueous $NaHCO_3$ (3 times with 10 mL), water (3 times with 10 mL) and aqueous NaCl (3 times with 100 mL). The organic phase was dried with Na_2SO_4 and evaporated under reduced pressure, obtaining methyl 2,4-dihydroxybenzoate **2** (19.3 g, yield 88%).

LC-UV purity: 98.01% (λ= 220 nm), > 99% (λ= 254 nm)

^{1}H-NMR (DMSO-d6) δ: 10.73 (s, 1 H), 10.49 (s, 1 H), 7,64 (dd, J=3.2, J=8.6, 1 H), 6.39 (d, J=8.6, 1 H), 6.32 (d, J=3.2, 1 H), 3.85 (s, 3H). ES- $[M-H]^-$ m/z 153.

*2,4-dihydroxybenzamide (**3**)*

Methyl 2,4-dihydroxybenzoate (**2**) (19.3 g, 115 mmol) was placed in a microwave reactor test-tube together with a 33% aqueous ammonia solution (20 mL). The mixture was irradiated with microwaves (250 W) at 120 °C for 30 minutes, then acidified with aqueous 1 N HCl and extracted with ethyl acetate (3 times with 100 mL). The collected organic phases were washed with aqueous

NaCl (twice with 100 mL), dried with Na_2SO_4 and evaporated under reduced pressure, obtaining 2,4-dihydroxybenzamide **3** (10.6 g, yield 60%).

LC-UV purity: 90.44% (λ= 220 nm), 89% (λ= 254 nm)

^{1}H-NMR (DMSO-d6) δ: 13.29 (s, 1 H), 10.08 (s, 1 H), 8.11 (s, 1 H), 7,66 (d, J=8.6, 1 H), 7.59 (s, 1 H), 6.29-6.18 (m, 2 H).

ES+ $[M+H]^+$; m/z 154.6.

*7-hydroxy-2,2-dimethyl-3H-1,3-benzoxazin-4-one (**4a**)*

2,4-dihydroxybenzamide (**3**) (5.0 g, 32.7 mmol) was dissolved in 40 mL of acetone together with 2,2-dimethoxypropane (40.0 mL, 325 mmol) and *para*-toluenesulfonic acid (catalytic), in a 250 mL flask held over a flame and placed under a nitrogen atmosphere. The mixture was left under agitation at room temperature for 10 hours, after which it was filtered in a Buchner funnel. The solid obtained was washed liberally with water and dried in a stove at 40 °C under reduced pressure, obtaining product (2) as a white solid (3.80 g, yield: 61%).

LC-UV purity: > 99% (λ= 220 nm), > 99% (λ= 254 nm)

^{1}H-NMR (DMSO d6) δ; 8.29 (s, 1 H), 7.56 (d, J= 8.6, 1 H), 6.46 (dd, J=2.2, J=8.6, 1 H), 6.26 (d, J=2.2, 1 H), 1 .49 (s, 6H).

ES+ $[M+H]^+$; m/z 194.6.

*7-hydroxyspiro[3H-1,3-benzoxazine-2,1'-cyclohexane]-4-one (**4b**)*

Compound **4b** was prepared according to the general procedure and isolated as a white solid in a 65% yield.

LC-UV purity: > 99% (λ= 220 nm), > 99% (λ= 254 nm)

^{1}H-NMR (DMSO-d6) δ: 10.23 (s, 1 H), 8.28 (s, 1 H), 7.54 (d, J=8.4 Hz, 1 H), 6.46 (dd, J=8.4 Hz, J=2.2 Hz 1 H), 6.29 (d, J=2.2 Hz 1 H), 1.96 (m, 2H), 1.55 (m, 7H), 1.22 (m, 1 H).

ES+ $[M+H]^+$; m/z 233.9.

*7-hydroxyspiro[3H-1,3-benzoxazine-2,4'-tetrahydropyran]-4-one (**4c**)*

Compound **4c** was prepared according to the general procedure and isolated as a white solid in a 57% yield.

LC-UV purity: > 99% (λ= 220 nm), > 99% (λ= 254 nm)

^{1}H-NMR (DMSO-d6) δ: 10.32 (s, 1 H), 8.44 (s, 1 H), 7.58 (d, J=8.4 Hz, 1 H), 6.50 (d, J=8.4 Hz, 1 H), 6.36 (s, 1 H), 3.75-3.58 (m, 4H), 1 .54 (br s, 7H), 1 .97-1.76 (m, 4 H). ES+ $[M+H]^+$; m/z 236.4.

General Procedures for the Preparation of compounds 5a-b (scheme 2 - step 1a)

*Synthesis of sulfonylated derivatives (**5a-b**)*

*(2,2-dimethyl-4-oxo-3H-1,3-benzoxazin-7-yl) naphthalene-1-sulfonate **(5a2)***

1.50 g of product (**4a**) (7.76 mmol) was dissolved in anhydrous DMF (30 mL) in a 100 mL flask held over a flame and placed under a nitrogen atmosphere. Potassium carbonate (1.18 g, 8.54 mmol) and 1-naphtylsulfonyl chloride (1.99 g, 8.54 mmol) were then added, and the mixture was left under agitation for 10 hours. The mixture was then concentrated under reduced pressure, recovered with DCM (100 mL) and washed with aqueous $NaHCO_3$ (3 times with 100 mL), water (3 times with 100 mL) and aqueous NaCl (3 times with 100 mL). The organic phase was dried with Na_2SO_4 and evaporated under reduced pressure, obtaining the intermediate (**5a2**) as a white solid (2.41 g, yield 81%).

LC-UV purity: > 99% (λ= 220 nm), > 99% (λ= 254 nm)

^{1}H NMR (400 MHz, DMSO-d6): δ 8.73 (s, 1H), 8.62 (d, J=8.7 Hz, 1H), 8.44 (d, J=8.3 Hz, 1H), 8.24-8.17 (m, 2H), 7.94-7.89 (m, 1H), 7.82-7.78 (m, 1H), 7.71-7.66 (m, 2H), 6.62 (dd, J=8.58 Hz, J=2.2 Hz, 1H), 6.46 (d, J=2.2 Hz, 1H), 1.44 (s, 6H).

^{13}C NMR (100 MHz, DMSO-d6): δ 160.39, 156.64, 153.24, 137.20, 134.21, 132.10, 130.02, 129.75, 129.48, 128.21, 125.14, 124.37, 116.75, 115.51, 110.56, 88.92, 79.52, 27.53.

ES+ $[M+H]^+$; m/z 384.2.

*(2,2-dimethyl-4-oxo-3H-1,3-benzoxazin-7-yl) 4-methylbenzenesulfonate (**5a3**)*

Product (**5a3**) was obtained from product (**4a**) by following a similar procedure to that described for product (**5a2**), using 4-methylbenzenesulfonyl chloride instead of 1-naphtylsulfonyl chloride.

LC-UV purity: 95% (λ= 220 nm), 96% (λ= 254 nm).

ES+ $[M+H]^+$; m/z 348.2.

*(2,2-dimethyl-4-oxo-3H-1,3-benzoxazin-7-yl) 4-phenoxybenzenesulfonate (**5a5**)*

Product (**5a5**) was obtained from product (**4a**) by following a similar procedure to that described for product (**5a2**), using 4-phenoxybenzenesulfonyl chloride instead of 1-naphtylsulfonyl chloride in a 72% yield.

LC-UV purity: 95% (λ= 220 nm), 98% (λ= 254 nm).

ES+ $[M+H]^+$; m/z 426.93

*(2,2-dimethyl-4-oxo-3H-1,3-benzoxazin-7-yl) 4-bromobenzenesulfonate (**5a6**)*

Product (**5a6**) was obtained from product (**4a**) by following a similar procedure to that described for product (**5a2**), using 4-bromobenzenesulfonyl chloride instead of 1-naphtylsulfonyl chloride in a 65% yield.

LC-UV purity: 96,83% (λ= 220 nm), 96% (λ= 254 nm).

ES+ $[M+H]^+$; m/z 414.83.

*(4-oxospiro[3H-1,3-benzoxazine-2,1'-cyclohexane]-7-yl) 2-nitrobenzenesulfonate (**5b1**)*

100 mg of product (**4b**) (0.429 mmol) was dissolved in anhydrous DMF (2 mL) in a 5 mL Schlenk tube, held over a flame and placed under a nitrogen atmosphere. Potassium carbonate (118 mg, 0.643 mmol) was added, and the mixture was left under agitation for 15 minutes. (2-nitro)-benzene-sulphonyl chloride (0.643 mmol) was then added, and the mixture was left under agitation for 10 hours. Aqueous Na_2CO_3 (3 mL) was added, and the mixture was extracted with ethyl acetate (3 times with 5 mL). The organic phases were collected and washed with water (3 times with 10 mL) and aqueous NaCl (3 times with 10 mL). The organic phase was dried with Na_2SO_4 and evaporated under reduced pressure. The residue was triturated with a mixture of CH_3CN/DMF in a 1:1 ratio, obtaining product (**5b1**) as a white solid (yield 34%).

LC-UV purity: > 99% (λ= 220 nm), > 99% (λ= 254 nm).

^{1}H NMR (400 MHz, DMSO-d6): δ 8.81 (s, 1H), 8.21 (dd, J=8.02 Hz, J=1.08 Hz, 1H), 8.11-8.02 (m, 2H), 7.92-7.88 (m, 1H), 7.79 (d, J=8.48 Hz, 1H), 6.90 (dd, J=8.48 Hz, J=2.32 Hz, 1H), 6.79 (d, J=2.32 Hz, 1H), 1.94 (d, J=12.89 Hz, 2H), 1.61-1.42 (m, 7H), 1.30-1.15 (m, 1H).

^{13}C NMR (100 MHz, DMSO-d6): δ 21.71, 24.47, 35.75, 89.21, 111.05, 115.98, 118.40, 125.84, 129.45, 132.17, 133.42, 137.69, 137.99, 148.72, 152.83, 156.60, 160.21.

ES+ $[M+H]^+$; m/z 419.2.

*(4-oxospiro[3H-1,3-benzoxazine-2,1'-cyclohexane]-7-yl) 3-methoxybenzenesulfonate (**5b2**)*

Product (**5b2**) was obtained from product (**4b**) by following a similar procedure to that described for product (**5b1**), using 3-methoxybenzenesulfonyl chloride instead of (2-nitro)-benzene-sulphonyl chloride (yield 45%).

LC-UV purity: 97% (λ= 220 nm), 95% (λ= 254 nm).

ES+ $[M+H]^+$; m/z 404.2.

*(4-oxospiro[3H-1,3-benzoxazine-2,1'-cyclohexane]-7-yl) 1-methylpyrazole-3-sulfonate (**5b3**)*

Product (**5b3**) was obtained from product (**4b**) by following a similar procedure to that described for product (**5b1**), using 3-methoxybenzenesulfonyl chloride instead of (2-nitro)-benzene-sulphonyl chloride (yield 57%).

LC-UV purity: > 99% (λ= 220 nm), 92% (λ= 254 nm).

ES+ $[M+H]^+$; m/z 379.2.

*3,4-dihydro-4-oxo-2H-benzo[e][1,3]oxazin-7-yl thiophene-2-sulfonate (**5b5**)*

Product (**5b5**) was obtained from product (**4b**) by following a similar procedure to that described for product (**5b1**), using thiophene-2-sulfonyl chloride instead of (2-nitro)-benzene-sulphonyl chloride (yield 58%).

LC-UV purity: > 99% (λ= 220 nm), > 99% (λ= 254 nm).

ES+ $[M+H]^+$; m/z 380.98

*Synthesis of alkylether derivatives (**5a-b**)*

582 *2,2-dimethyl-7-[[4-(trifluoromethoxy)phenyl]methoxy]-3H-1,3-benzoxazin-4-one (**5a1**)*

583 Compound (**4a**) (100 mg, 0.518 mmol) was dissolved in anhydrous DMF (2 mL) in a 5 mL Schlenk
584 tube held over a flame and placed under a nitrogen atmosphere. Potassium carbonate (118 mg, 0.64
585 mmol) was added, and the mixture was left under agitation for 15 minutes. 4-trifluoromethylbenzyl
586 bromide (145 mg, 0.57 mmol) was then added, and the mixture was left under agitation for 10
587 hours. Aqueous NH_4Cl (3 mL) was added, and the mixture was extracted with ethyl acetate (3 times
588 with 5 mL). The collected organic phases were washed with water (3 times with 10 mL) and
589 aqueous NaCl (3 times with 10 mL). The organic phase was dried with Na_2SO_4 and evaporated
590 under reduced pressure. Thus, product (**5a1**) was obtained as a white solid (177 mg, yield 93%).
591 LC-UV purity: 97% (λ= 220 nm), 97% (λ= 254 nm).
592 ES+ [M+H]+; m/z 368.9.
593 *7-(3,3-dimethyl-2-oxo-butoxy)-2,2-dimethyl-3H-1,3-benzoxazin-4-one (**5a4**)*
594 Product (**5a4**) was obtained from product (**4a**) by following a similar procedure to that described for
595 product (**5a1**), using 1-chloro-3,3-dimethylbutan-2-one instead of 4-trifluoromethylbenzyl bromide
596 in a 89% yield.
597 LC-UV purity: 97% (λ= 220 nm), 97% (λ= 254 nm).
598 ES+ $[M+H]^+$; m/z 292.85.
599 *7-[(3-methoxyphenyl)methoxy]-2,2-dimethyl-3H-1,3-benzoxazin-4-one (**5a7**)*
600 Product (**5a7**) was obtained from product (**4a**) by following a similar procedure to that described for
601 product (**5a1**), using pivaloyl chloride instead of 4-trifluoromethylbenzyl bromide in a 79% yield.
602 LC-UV purity: >99% (λ= 220 nm), >99% (λ= 254 nm).
603 ES+ $[M+H]^+$; m/z 314.84.
604 *7-[[4-(trifluoromethoxy)phenyl]methoxy]spiro[3H-1,3-benzoxazine-2,1'-cyclohexane]-4-one (**5b4**)*
605 Product (**5b4**) was obtained from product (**4b**) by following a similar procedure to that described
606 for product (**5a1**), using 4-(trifluoromethoxy)benzyl bromide instead of 4-trifluoromethylbenzyl
607 bromide in a 88% yield.

608 LC-UV purity: 95% (λ= 220 nm), 95% (λ= 254 nm).

609 ES+ $[M+H]^+$; m/z 409.08.

610 **General Procedures for the Preparation of Compounds 6b-c (scheme2 – step1b)**

611 *3-benzyl-7-hydroxy-spiro[1,3-benzoxazine-2,1'-cyclohexane]-4-one (**6b**)*

612 3.00 g of compound (**4b**) (12.9 mmol) were dissolved in anhydrous DMF (10 mL) in a 50 mL flask
613 held over a flame and placed under a nitrogen atmosphere. Potassium carbonate (5.33 g, 38.6
614 mmol) was then added, and after cooling the mixture to 0 °C with an ice bath,
615 chloromethoxymethane (MOMCI - 1.95 mL, 25.7 mmol) was added drop by drop. The mixture was
616 left under agitation for 10 hours at room temperature, after which it was poured into a saturated
617 aqueous solution of sodium carbonate (20 mL) and ice. The mixture was extracted with ethyl
618 acetate (3 times with 30 mL). The organic phases were collected and washed with water (3 times
619 with 20 mL) and aqueous NaCl (3 times with 20 mL), dried with Na_2SO_4 and evaporated under
620 reduced pressure, thus obtaining the MOM protected intermediate as a pink solid
621 The crude was dissolved in anhydrous DMF (100 mL) in a 250 mL flask held over a flame and
622 placed under a nitrogen atmosphere. The mixture, placed under agitation, was cooled to 0 °C with
623 an ice bath, and then sodium hydride (521 mg, 21.7 mmol) and benzyl bromide (1.9 mL, 16.3
624 mmol) were added. The mixture was left under agitation at room temperature for 10 hours, then
625 acidified with NH_4Cl aq. s.s. and extracted with ethyl acetate (3 times with 20 mL). The organic
626 phases were collected and washed with aqueous NaCl (3 times with 20 mL), dried with Na_2SO_4 and
627 evaporated under reduced pressure. The residue was purified with a silica column, using as an
628 eluent an ether mixture of petroleum/ethyl acetate at a ratio of 9:1, obtaining the MOM protected
629 benzyl derivative as a white solid.
630 Finally the intermediate dissolved in methanol (50 mL) and aqueous 6M HCl (4 mL). The mixture
631 was left under agitation at room temperature for 10 hours. The mixture was then concentrated under
632 reduced pressure, recovered with ethyl acetate (100 mL) and washed with aqueous NaCl (3 times

633 with 100 mL). The organic phase was dried with Na_2SO_4 and evaporated under reduced pressure,
634 obtaining product (**6b**) as a white solid (3.0 g, yield 69.9%).
635 LC-UV purity: > 95% (λ= 220 nm), > 95% (λ= 254 nm).
636 ^{1}H-NMR (DMSO-d6) δ: 10.39 (br s, 1H), 7.65 (d, J=8.4 Hz, 1 H), 7.34-7.20 (m, 5H), 6.55 (dd,
637 J=8.4 Hz, J=2.2 Hz, 1 H), 6.37 (d, J=2.2 Hz, 1 H), 4.76 (s, 2H), 1.94-1.90 (m, 2H); 1.69-1.5 (m,
638 7H), 1.17-1.10(m 1H).
639 ES+ $[M+H]^+$; m/z 323.9.
640 *3-benzyl-7-hydroxy-spiro[1,3-benzoxazine-2,4'-tetrahydropyran]-4-one (**6c**)*
641 Product (**6c**) was obtained from product (**4c**) by following a similar procedure to that described for
642 product (**6b**) in a 72% yield.
643 LC-UV purity: > 95% (λ= 220 nm), > 95% (λ= 254 nm).
644 ^{1}H-NMR (DMSO-d6) δ: 10.42 (s, 1H), 7.68 (d, J=8.5 Hz, 1 H), 7.36-7.24 (m, 5H), 6.57 (dd, J=8.5
645 Hz, J=2.2 Hz, 1 H), 6.46 (d, J=2.2 Hz, 1 H), 4.76 (s, 2H), 3.73-3.68 (m, 2H), 3.60-3.54 (m, 2H),
646 1.99-1.83 (m, 4H).
647 ES+ $[M+H]^+$; m/z 325.9.
648 **General Procedures for the Preparation of Target Compounds 7a1-8, 7b1-5 (Scheme 2 - Step**
649 **2a)**
650 *(3-benzyl-4-oxo-spiro[1,3-benzoxazine-2,1'-cyclohexane]-7-yl) thiophene-2-sulfonate (**7b5**)*
651 Compound (**5b5**) (46 mg, 0.121 mmol) was dissolved in anhydrous DMF (2 mL) in a 5mL Schlenk
652 tube held over flame and placed under nitrogen atmosphere. The mixture was cooled to 0 °C with
653 an ice bath and sodium hydride (3.2 mg, 0.133 mmol) and benzyl bromide (17.3 mL, 0,145 mmol).
654 were then added (3 mL). The mixture was left under agitation for 10 hours. Aqueous HCl 1N was
655 added, and the mixture was extracted with ethyl acetate (3 times with 5 mL). The collected organic
656 phases were washed with aqueous NaCl (3 times with 5 mL). The organic phase was dried with
657 Na_2SO_4 and evaporated under reduced pressure. The obtained residue was purified by means of

semi-preparative HPLC (eluent CH_3CN 10 to 80% in H_20), obtaining product (**7b5**) as a waxy solid (45.0 mg, yield 79%).

LC-UV purity: > 99% (λ= 220 nm), > 99% (λ= 254 nm).

^{1}H NMR (400 MHz, DMSO-d6): δ 8.24 (dd, J=5.01 Hz, J=1.18 Hz, 1H), 7.90-7.84 (m, 2H), 7.35-7.22 (m, 6H), 6.91 (dd, J=8.61 Hz, J=2.18 Hz, 1H), 6.79 (d, J=2.18 Hz, 1H), 4.80 (s, 2H), 1.89-1.36 (m, 9H), 1.17-1.05 (m, 1H).

^{13}C NMR (100 MHz, DMSO-d6): δ 160.75, 155.15, 153.27, 139.33, 138.21, 137.44, 132.71, 129.86, 129.10, 128.92, 127.38, 127.34, 117.84, 116.61, 111.34, 93.59, 43.98, 33.43, 24.09, 22.06.

ES+ $[M+H]^+$; m/z 470.2.

*3-[(4-fluorophenyl)methyl]-2,2-dimethyl-7-[[4-(trifluoromethoxy)phenyl]methoxy]-1,3-benzoxazin-4-one (**7a1**)*

Product (**7a1**) was obtained from product (**5a1**) by following a similar procedure to that described for product (**7b5**), using 4-fluorobenzenyl bromide instead of benzyl bromide (15.6 mg, yield 73%).

LC-UV purity: 98% (λ= 220 nm), 98% (λ= 254 nm).

^{1}H NMR (400 MHz, DMSO-d6): δ 7.76 (d, J=8.68 Hz, 1H), 7.61-7.59 (m, 2H), 7.42-7.40 (m, 2H), 7.36-7.32 (m, 2H), 7.18-7.13 (m, 2H), 6.79 (dd, J=8.64 Hz, J=2.30 Hz, 1H), 6.64 (d, J=2.30 Hz, 1H), 5.20 (s, 1H), 4.74 (s, 2H), 1.51 (s, 6H).

^{13}C NMR (100 MHz, DMSO-d6): δ 163.71, 161.49, 156.64, 148.48, 136.39, 135.87, 130.26, 129.61, 129.51, 129.43, 121.60, 115.78, 115.57, 110.74, 110.40, 102.38, 92.68, 69.20, 43.65, 25.99.

ES+ $[M+H]^+$; m/z 477.2.

*(2,2,3-trimethyl-4-oxo-1,3-benzoxazin-7-yl) naphthalene-1-sulfonate (**7a2**)*

Product (**7a2**) was obtained from product (**5a2**) by following a similar procedure to that described for product (**7b5**), using methyl iodide instead of benzyl bromide, as yellow oil (12.1 mg, yield 83%).

LC-UV purity: 99% (λ= 220 nm), 99% (λ= 254 nm).

^{1}H NMR (400 MHz, DMSO-d6): δ 8.62 (d, J=8.60 Hz, 1H), 8.44 (d, J=8.33 Hz, 1H), 8.23-8.17 (m, 2H), 7.93-7.89 (m, 1H), 7.82-7.78 (m, 1H), 7.70-7.67 (m, 2H), 6.65 (dd, J=8.57 Hz, J=2.32 Hz), 6.48 (d, J=2.20 Hz, 1H), 2.93 (s, 1H), 1.51 (s, 6H).

^{13}C NMR (100 MHz, DMSO-d6): δ 159.76, 155.50, 153.11, 137.20, 134.20, 132.10, 130.02, 130.01, 129.77, 129.72, 128.21, 127.97, 125.14, 124.36, 116.63, 115.80, 110.47, 92.79, 27.60, 25.03.

ES+ $[M+H]^{+}$; m/z 399.0.

*[3-[(4-fluorophenyl)methyl]-2,2-dimethyl-4-oxo-1,3-benzoxazin-7-yl] 4-methylbenzenesulfonate (**7a3**)*

Product (**7a3**) was obtained from product (**5a3**) by following a similar procedure to that described for product (**7b5**), using 4-fluorobenzenyl bromide instead of benzyl bromide, as colourless oil (25.5 mg, yield 88%).

LC-UV purity: 99% (λ= 220 nm), 99% (λ= 254 nm)

^{1}H NMR (400 MHz, DMSO-d6): δ 7.85-7.77 (m, 3H), 7.50 (d, J=7.99 Hz, 2H), 7.35-7.31 (m, 2H), 7.18-7.13 (m, 2H), 6.83 (dd, J=8.53 Hz, J=2.20 Hz, 1H), 6.69 (d, J=2.20 Hz, 1H), 4.74 (s, 2H), 2.43 (s, 3H), 1.49 (s, 6H).

^{13}C NMR (100 MHz, DMSO-d6): δ 194.61, 161.42, 146.66, 144.00, 131.47, 130.80, 129.58, 129.50, 128.81, 120.48, 115.85, 115.64, 111.17, 99.99, 93.37, 88.78, 43.91, 25.93, 21.65.

ES+ $[M+H]^{+}$; m/z 457.1.

*3-benzyl-7-(3,3-dimethyl-2-oxo-butoxy)-2,2-dimethyl-1,3-benzoxazin-4-one (**7a4**)*

Product (**7a4**) was obtained from product (**5a4**) by following a similar procedure to that described for product (**7b5**), as waxy solid (23.2 mg, yield 67%).

LC-UV purity: 99% (λ= 220 nm), 99% (λ= 254 nm)

^{1}H NMR (400 MHz, DMSO-d6): δ 7.73 (d, J=8.65 Hz, 1H), 7.35-7.23 (m, 5H), 6.67 (dd, J=8.65 Hz, J=2.40 Hz, 1H), 6.51 (d, J=2.40 Hz, 1H), 5.21 (s, 2H), 4.76 (s, 2H), 1.51 (s, 6H), 1.17 (s, 9H).

^{13}C NMR (100 MHz, DMSO-d6): δ 209.71, 163.55, 161.45, 156.53, 139.70, 129.42, 128.91, 127.36, 110.70, 110.17, 102.16, 92.62, 88.78, 69.22, 44.32, 42.46, 26.19, 26.00.

ES+ $[M+H]^+$; m/z 383.1.

*(2,2,3-trimethyl-4-oxo-1,3-benzoxazin-7-yl) 4-phenoxybenzenesulfonate (7**a5**)*

Product (**7a5**) was obtained from product (**5a5**) by following a similar procedure to that described for product (**7b5**), using methyl iodide instead of benzyl bromide, as colourless oil (25.0 mg, yield 70%).

LC-UV purity: 99% (λ= 220 nm), 99% (λ= 254 nm).

^{1}H NMR (400 MHz, DMSO-d6): δ 7.88-7.84 (m, 2H), 7.78 (d, J=8.55 Hz, 1H), 7.52-7.48 (m, 2H), 7.33-7.29 (m, 1H), 7.19-7.14 (m, 4H), 6.81 (dd, J=8.52 Hz, J=2.2 Hz), 6.66 (d, J=2.20 Hz, 1H), 2.97 (s, 1H), 1.57 (s, 1H).

^{13}C NMR (100 MHz, DMSO-d6): δ 163.15, 159.92, 155.57, 154.64, 153.22, 131.65, 131.02, 129.70, 127.60, 125.97, 120.91, 118.19, 116.63, 116.33, 111.14, 92.79, 27.64, 25.11.

ES+ $[M+H]^+$; m/z 441.1.

*(2,2,3-trimethyl-4-oxo-1,3-benzoxazin-7-yl) 4-phenoxybenzenesulfonate (7**a6**)*

Product (**7a6**) was obtained from product (**5a6**) by following a similar procedure to that described for product (**7b5**), using N-(chloromethyl)-N-methyl-acetamide instead of benzyl bromide, as colourless oil (18.0 mg, yield 65%).

LC-UV purity: 95% (λ= 220 nm), 95% (λ= 254 nm).

^{1}H NMR (400 MHz, DMSO-d6): δ 7.91-7.89 (m, 2H), 7.86-7.75 (m, 3H), 6.81 (dd, J=2.28 Hz, J=8.44 Hz, 1H), 6.72 (d, J=2.28 Hz, 1H), 4.36 (s, 2H), 3.03 (s, 3H), 2.84 (s, 3H), 1.57 (s, 6H).

^{13}C NMR (100 MHz, DMSO-d6): 167.74, 162.40, 159.63, 155.87, 153.09, 133.52, 130.75, 130.07, 129.77, 117.04, 116.34, 111.28, 93.09, 43.63, 36.35, 35.76, 25.79.

ES+ $[M+H]^+$; m/z 498.1.

*3-[(4-isopropylphenyl)methyl]-7-[(3-methoxyphenyl)methoxy]-2,2-dimethyl-1,3-benzoxazin-4-one (7**a7**)*

Product (**7a7**) was obtained from product (**5a7**) by following a similar procedure to that described for product (**7b5**), using 1-(bromomethyl)-4-isopropylbenzene instead of benzyl bromide, as colourless oil (12.0 mg, yield 38%).

LC-UV purity: 99% (λ= 220 nm), 99% (λ= 254 nm).

^{1}H NMR (400 MHz, DMSO-d6): δ 7.75 (d, 8.67 Hz, 1H), 7.32 (t, J=8.04 Hz, 1H), 7.22-7.11 (m, 4H), 7.03-7.01 (m, 2H), 6.93-6.90 (m, 1H), 6.77 (dd, J=2.34 Hz, J=8.66 Hz, 1H), 6.61 (d, J=2.34 Hz, 1H), 5.14 (s, 2H), 4.70 (s, 2H), 3.76 (s, 3H), 2.85 (sept, J=6.90 Hz, 1H), 1.15 (s, 6H), 1.18 (d, J=6.90 Hz, 6H).

^{13}C NMR (100 MHz, DMSO-d6): δ 23.92, 25.99, 43.64, 55.54, 56.02, 70.01, 92.66, 102.36, 110.45, 110.61, 113.80, 113.92, 115.56, 115.78, 120.35, 129.42, 129.50, 129.55, 130.11, 138.41, 156.61, 159.82, 161.51, 163.87.

ES+ $[M+H]^{+}$; m/z 447.2.

3-[(4-fluorophenyl)methyl]-7-[(3-methoxyphenyl)methoxy]-2,2-dimethyl-1,3-benzoxazin-4-one

(7a8)

Product (**7a8**) was obtained from product (**5a7**) by following a similar procedure to that described for product (**7b5**), using 4-fluorobenzenyl bromide instead of benzyl bromide, as colourless oil (26.3 mg, yield 77%).

LC-UV purity: 99% (λ= 220 nm), 99% (λ= 254 nm).

^{1}H NMR (400 MHz, DMSO-d6): δ 7.75 (d, J=8.67 Hz, 1H), 7.36-7.30 (m, 3H), 7.18-7.13 (m, 2H), 7.03-7.01 (m, 2H), 6.93-6.90 (m, 1H), 6.78 (dd, J=8.64 Hz, J=2.33 Hz, 1H), 6.61 (d, J=2.30 Hz, 1H), 5.14 (s, 2H), 4.73 (s, 2H), 3.76 (s, 3H), 1.51 (s, 6H).

^{13}C NMR (100 MHz, DMSO-d6): δ 163.87, 161.51, 159.82, 156.61, 138.41, 130.11, 129.55, 129.50, 129.42, 120.35, 115.78, 115.56, 113.92, 113.80, 110.61, 110.45, 102.36, 92.66, 70.01, 55.54, 43.64, 25.99.

ES+ $[M+H]^{+}$; m/z 423.1.

*[3-[(4-isopropylphenyl)methyl]-4-oxo-spiro[1,3-benzoxazine-2,1'-cyclohexane]-7-yl] 3-methoxybenzenesulfonate (**7b1**)*

Product (**7b1**) was obtained from product (**5b2**) by following a similar procedure to that described for product (**7b5**), using 1-(bromomethyl)-4-isopropylbenzene instead of benzyl bromide, as waxy solid (28.0 mg, yield 77%).

LC-UV purity: 99% (λ= 220 nm), 99% (λ= 254 nm).

^{1}H NMR (400 MHz, DMSO-d6): δ 7.85 (d, J=8.46 Hz, 1H), 7.58 (t, J=8.08 Hz, 1H), 7.45-7.38 (m, 2H), 7.34-7.33 (m, 1H), 7.18 (s, 4H), 6.91 (dd, J=2.22 Hz, J=8.52 Hz, 1H), 6.79 (d, J=2.22 Hz, 1H), 4.74 (s, 2H), 3.83 (s, 2H), 2.84 (sept, J=6.68 Hz, 1H), 1.87-1.69 (m, 4H), 1.54-1.40 (m, 5H), 1.23-1.14 (m, 7H).

^{13}C NMR (100 MHz, DMSO-d6): δ 160.70, 160.13, 155.09, 153.26, 147.39, 136.66, 135.31, 131.55, 129.80, 127.26, 126.78, 121.92, 120.94, 117.66, 116.60, 113.11, 111.34, 93.54, 56.33, 43.75, 33.48, 33.40, 24.34, 24.09, 22.04.

ES+ $[M+H]^{+}$; m/z 537.3.

*[3-(4-cyanobutyl)-4-oxo-spiro[1,3-benzoxazine-2,1'-cyclohexane]-7-yl] 3-methoxybenzenesulfonate (**7b2**)*

Product (**7b2**) was obtained from product (**5b2**) by following a similar procedure to that described for product (**7b5**), using 5-bromopentanenitrile instead of benzyl bromide, as waxy solid (19.6 mg, yield 63%).

LC-UV purity: 96% (λ= 220 nm), 99% (λ= 254 nm).

^{1}H NMR (400 MHz, DMSO-d6): δ 7.77 (d, J=8.55 Hz, 1H), 7.58 (t, J=8.15 Hz, 1H), 7.43-7.37 (m, 2H), 7.32-7.31 (m, 1H), 6.86 (dd, J=2.20 Hz, J=8.50 Hz, 1H), 6.75 (d, J=2.20 Hz, 1H), 3.82 (s, 3H), 3.49 (t, J=7.60 Hz, 2H), 2.54 (t, J=6.65 Hz, 2H), 2.00-1.97 (m, 2H), 1.83-1.75 (m, 2H), 1.67-1.42 (m, 9H), 1.30-1.19 (m, 1H).

^{13}C NMR (100 MHz, DMSO-d6): δ 16.21, 21.92, 22.5, 24.12, 29.03, 33.33, 40.32, 56.43, 93.52, 111.07, 112.91, 116.17, 120.57, 121.27, 121.85, 129.37, 131.35, 131.42, 135.54, 153.52, 153.81, 155.04, 150.21.

ES+ $[M+H]^+$; m/z 486.2.

*[3-[(4-cyanophenyl)methyl]-4-oxo-spiro[1,3-benzoxazine-2,1'-cyclohexane]-7-yl] 1-methylpyrazole-3-sulfonate (**7b3**)*

Product (**7b3**) was obtained from product (**5b3**) by following a similar procedure to that described for product (**7b5**), using 4-(bromomethyl)benzonitrile instead of benzyl bromide, as waxy solid (27.1 mg, yield 81%).

LC-UV purity: 98% (λ= 220 nm), 99% (λ= 254 nm).

^{1}H NMR (400 MHz, DMSO-d6): δ 8.05 (d, J=2.30 Hz, 1H), 7.87-7.79 (m, 3H), 7.46 (d, J=8.29, 2H), 6.93-6.88 (m, 3H), 4.89 (s, 2H), 3.99 (s, 3H), 1.88-1.44 (m, 9H), 1.24-1.11 (m, 1H).

^{13}C NMR (100 MHz, DMSO-d6): δ 21.94, 23.99, 33.07, 40.25, 43.80, 93.50, 109.31, 111.06, 116.42, 119.10, 121.86, 123.82, 128.11, 129.80, 132.93, 134.50, 144.12, 145.71, 154.73, 158.47, 161.11.

ES+ $[M+H]^+$; m/z 494.2.

*4-[[4-oxo-7-[[4-(trifluoromethoxy)phenyl]methoxy]spiro[1,3-benzoxazine-2,1'-cyclohexane]-3-yl]methyl]benzonitrile(**7b4**)*

Product (**7b4**) was obtained from product (**5b4**) by following a similar procedure to that described for product (**7b5**), using 4-(bromomethyl)benzonitrile instead of benzyl bromide, as waxy solid (41.2 mg, yield 72%).

LC-UV purity: 98% (λ= 220 nm), 99% (λ= 254 nm)

^{1}H NMR (400 MHz, DMSO-d6): δ 7.81-7.75 (m, 3H), 7.58-7.46 (m, 5H), 7.36-7.34 (m, 1H), 6.81 (dd, J=8.54 Hz, J=2.42 Hz, 1H), 6.75 (d, J=2.33 Hz, 1H), 5.26 (s, 2H), 4.87 (s, 2H), 1.92-1.89 (m, 2H), 1.75-1.54 (m, 7H), 1.22-1.15 (m, 1H).

^{13}C NMR (100 MHz, DMSO-d6): δ 163.62, 161.67, 156.04, 148.93, 145.84, 139.73, 132.86, 131.02, 129.49, 128.15, 127.18, 120.93, 120.51, 119.30, 111.39, 110.62, 110.05, 102.71, 93.01, 69.13, 43.63, 33.34, 24.17, 22.12.

ES+ $[M+H]^+$; m/z 523.2.

General Procedures for the Preparation of Target Compounds 7b5-12 and 7c1-3 (scheme 2 – step 2b)

*(3-benzyl-4-oxo-spiro[1,3-benzoxazine-2,1'-cyclohexane]-7-yl) 4-methoxybenzenesulfonate (**7b8**)*

Product (**6b**) (70 mg, 0.22 mmol) was dissolved in anhydrous DMF (2 mL) in a 5 mL Schlenk tube held over a flame and placed under a nitrogen atmosphere. Potassium carbonate (61 mg, 0.44 mmol) was added and the mixture was left under agitation for 15 minutes. *p*-methoxybenzene-sulfonyl chloride (91 mg, 0.44 mmol) was then added and the mixture was left under agitation for 10 hours. A saturated solution of aqueous Na_2CO_3 (3 mL) was added and the mixture was extracted with ethyl acetate (3 times with 5 mL). The organic phases were collected and washed with water (3 times with 10 mL) and aqueous NaCl (3 times with 10 mL). The organic phase was dried with Na_2SO_4 and evaporated under reduced pressure. The obtained residue was purified by means of semi-preparative HPLC (eluent CH_3CN 10 to 80% in H_20), obtaining product (**7b8**) as a yellow solid (10.7 mg, yield 44%).

LC-UV purity: > 99% (λ= 220 nm), 93% (λ= 254 nm).

^{1}H NMR (400 MHz, DMSO-d6): δ 7.85-7.79 (m, 3H), 7.34-7.24 (m, 5H), 7.18-7.15 (m, 2H), 6.87 (dd,, J=2.20 Hz, J=8.51 Hz, 1H), 6.73 (d, J=2.20 Hz, 1H), 4.79 (s, 2H), 3.86 (s, 3H), 1.86-1.83 (m, 2H), 1.73-1.65 (m, 2H), 1.57-1.36 (m, 5H), 1.16-1.10 (m, 1H).

^{13}C NMR (100 MHz, DMSO-d6): δ 22.08, 24.04, 33.42, 43.81, 56.12, 92.70, 111.52, 115.55, 116.68, 116.81, 117.49, 125.80, 127.47, 128.84, 129.80, 130.92, 131.17, 139.20, 154.63, 160.60, 165.10.

ES+ $[M+Na]^+$; m/z 516.0.

*(3-benzyl-4-oxo-spiro[1,3-benzoxazine-2,1'-cyclohexane]-7-yl) thiophene-2-sulfonate (**7b5**)*

Product (**7b5**) was obtained from product (**6b**) by following a similar procedure to that described for product (**7b8**), using 2-thiophenesulfonyl chloride instead of *p*-methoxybenzene-sulfonyl chloride (13.4 mg, yield 61%).

LC-UV purity: > 99% (λ= 220 nm), > 99% (λ= 254 nm).

^{1}H NMR (400 MHz, DMSO-d6): δ 8.24 (dd, J=5.01 Hz, J=1.18 Hz, 1H), 7.90-7.84 (m, 2H), 7.35-7.22 (m, 6H), 6.91 (dd, J=8.61 Hz, J=2.18 Hz, 1H), 6.79 (d, J=2.18 Hz, 1H), 4.80 (s, 2H), 1.89-1.36 (m, 9H), 1.17-1.05 (m, 1H).

^{13}C NMR (100 MHz, DMSO-d6): δ 160.75, 155.15, 153.27, 139.33, 138.21, 137.44, 132.71, 129.86, 129.10, 128.92, 127.38, 127.34, 117.84, 116.61, 111.34, 93.59, 43.98, 33.43, 24.09, 22.06.

ES+ $[M+H]^{+}$; m/z 470.2.

*3-benzyl-4-oxo-spiro[1,3-benzoxazine-2,1'-cyclohexane]-7-yl) 4-(4-chlorophenyl)benzenesulfonate (7**b6**)*

Product (**7b6**) was obtained from product (**6b**) by following a similar procedure to that described for product (**7b8**), using 4-(4-chlorophenyl)benzenesulfonyl chloride instead of *p*-methoxybenzene-sulfonyl chloride, as white solid (12.7 mg, yield 58%).

LC-UV purity: 98% (λ= 220 nm), 99% (λ= 254 nm)

^{1}H NMR (400 MHz, DMSO-d6): δ 8.00-7.95 (m, 4H), 7.87 (d, J=8.55 Hz, 1H), 7.81-7.79 (m, 2H), 7.60-7.58 (m, 2H), 7.33-7.21 (m, 5H), 6.95 (dd, J=2.22 Hz, J=8.55 Hz, 1H), 6.76 (d, J=2.22 Hz, 1H), 4.78 (s, 2H), 1.84-1.81 (m, 2H), 1.70-1.63 (m, 2H), 1.41-1.30 (m, 5H), 1.10-1.02 (m, 1H).

^{13}C NMR (100 MHz, DMSO-d6): 162.40, 160.75, 155.10, 153.22, 145.59, 139.33, 137.03, 134.55, 133.08, 129.90, 129.67, 129.60, 129.52, 128.90, 128.35, 127.36, 127.31, 117.67, 116.75, 111.49, 93.52, 43.93, 33.38, 24.02, 22.03.

ES+ $[M+H]^{+}$; m/z 575.3.

*(3-benzyl-4-oxo-spiro[1,3-benzoxazine-2,1'-cyclohexane]-7-yl) 3-cyanobenzenesulfonate (7**b7**)*

Product (**7b7**) was obtained from product (**6b**) by following a similar procedure to that described for product (**7b8**), using (3-cyano)-benzene-sulphonyl chloride instead of *p*-methoxybenzene-sulfonyl chloride, as yellow waxy solid (11.3 mg, yield 55%).

LC-UV purity: 99% (λ= 220 nm), 92% (λ= 254 nm)

^{1}H NMR (400 MHz, DMSO-d6): δ 8.46 (s, 1H), 8.33-8.31 (m, 1H), 8.21-8.19 (m, 1H), 7.90-7.86 (m, 2H), 7.34-7.24 (m, 5H), 6.96 (dd, J=2.35 Hz, J=8.59 Hz, 1H), 6.89 (d, J=2.35 Hz, 1H), 4.80 (s, 2H), 1.87-1.84 (m, 2H), 1.73-1.67 (m, 2H), 1.58-1.36 (m, 5H), 1.17-1.07 (m, 1H).

^{13}C NMR (100 MHz, DMSO-d6): 22.11, 24.17, 33.40, 44.08, 94.21, 107.01, 111.77, 116.58, 118.51, 121.82, 127.51, 127.72, 127.83, 127.92, 128.43, 128.80, 129.17, 130.01, 131.76, 136.62, 152.23, 156.34, 164.71.

ES+ $[M+Na]^{+}$; m/z 511.2.

*(3-benzyl-4-oxo-spiro[1,3-benzoxazine-2,1'-cyclohexane]-7-yl) 4-cyanobenzenesulfonate (**7b9**)*

Product (**7b9**) was obtained from product (**6b**) by following a similar procedure to that described for product (**7b8**), using (4-cyano)-benzene-sulphonyl chloride instead of *p*-methoxybenzene-sulfonyl chloride, as white solid (12.4 mg, yield 57%).

LC-UV purity: 99% (λ= 220 nm), 92% (λ= 254 nm).

^{1}H NMR (400 MHz, DMSO-d6): δ 8.18-8.16 (m, 2H), 8.09-8.07 (m, 2H), 7.87 (d, J=8.53 Hz, 1H), 7.34-7.24 (m, 5H), 6.93 (dd,, J=2.22 Hz, J=8.51 Hz, 1H), 6.83 (d, J=2.22 Hz, 1H), 4.79 (s, 2H), 1.87-1.83 (m, 2H), 1.74-1.66 (m, 2H), 1.57-1.35 (m, 5H), 1.16-1.07 (m, 1H).

^{13}C NMR (100 MHz, DMSO-d6): δ 21.94, 24.17, 33.26, 43.99, 94.21, 111.02, 111.59, 116.29, 117.52, 118.12, 127.31, 127.72, 128.79, 129.59, 130.03, 134.23, 138.12, 139.49, 152.96, 155.10, 160.71.

ES+ $[M+H]^{+}$; m/z 489.1.

*(3-benzyl-4-oxo-spiro[1,3-benzoxazine-2,1'-cyclohexane]-7-yl) 1-methylimidazole-4-sulfonate (**7b10**)*

Product (**7b10**) was obtained from product (**6b**) by following a similar procedure to that described for product (**7b8**), using 1-methylimidazole-4-sulfonyl chloride instead of *p*-methoxybenzene-sulfonyl chloride, as white solid (13.0 mg, yield 57%)..

LC-UV purity: 99% (λ= 220 nm), 98% (λ= 254 nm).

^{1}H NMR (400 MHz, DMSO-d6): δ 8.10-8.09 (m, 1H), 8.00-7.99 (m, 1H), 7.85 (d, J=8.51 Hz, 1H), 7.34-7.22 (m, 5H), 6.89 (dd, J=2.22 Hz, J=8.51 Hz, 1H), 6.72 (d, J=2.22 Hz, 1H), 4.80 (s, 2H), 3.70 (s, 3H), 1.90-1.87 (m, 2H), 1.76-1.68 (m, 2H), 1.60-1.42 (m, 5H), 1.18-1.07 (m, 1H).

^{13}C NMR (100 MHz, DMSO-d6): 160.85, 155.03, 153.75, 141.61, 139.41, 133.10, 129.68, 129.39, 128.91, 127.35, 127.29, 117.30, 116.60, 111.20, 93.49, 43.93, 34.29, 33.44, 24.10, 22.05.

ES+ [M+H]+; m/z 468.2.

*(3-benzyl-4-oxo-spiro[1,3-benzoxazine-2,1'-cyclohexane]-7-yl) phenylmethanesulfonate (**7b11**)*

Product (**7b11**) was obtained from product (**6b**) by following a similar procedure to that described for product (**7b8**), using benzylsulfonyl chloride instead of *p*-methoxybenzene-sulfonyl chloride, as white solid (11.7 mg, yield 53%)..

LC-UV purity: 94%(λ= 220 nm), 98% (λ= 254 nm)

^{1}H NMR (400 MHz, DMSO-d6): δ 7.85 (d, J=8.59 Hz, 1H), 7.78-7.76 (m, 2H), 7.48 (d, J=8.12 Hz, 2H), 7.34-7.22 (m, 6H), 6.88 (dd, J=8.48 Hz, J=2.28 Hz, 1H), 6.72 (d, J=2.28 Hz, 1H), 4.79 (s, 2H), 2.42 (s, 2H), 1.85 (d, J=12.88 Hz, 2H), 1.70 (td, J=12.88 Hz, J=4.03 Hz, 2H), 1.58-1.34 (m, 5H), 1.18-1.07 (m, 1H).

^{13}C NMR (100 MHz, DMSO-d6): δ 217.62, 194.61, 162.41, 146.65, 144.00, 139.40, 130.78, 128.92, 128.85, 127.38, 127.33, 121.00, 111.53, 102.58, 99.99, 88.78, 47.38, 33.41, 28.96, 22.03, 21.65.

ES+ $[M+H]^{+}$; m/z 478.2.

*(3-benzyl-4-oxo-spiro[1,3-benzoxazine-2,1'-cyclohexane]-7-yl) 3-methoxybenzenesulfonate (**7b12**)*

Product (**7b12**) was obtained from product (**6b**) by following a similar procedure to that described for product (**7b8**), using (3-methoxy)-benzene-sulfonyl chloride instead of *p*-methoxybenzene-sulfonyl chloride, as waxy solid (14.8 mg, yield 60%)..

LC-UV purity: 99% (λ= 220 nm), 99% (λ= 254 nm)

^{1}H NMR (400 MHz, DMSO-d6): δ 7.86 (d, J=8.55 Hz, 1H), 7.59 (t, J= 8.09 Hz, 1H), 7.45-7.38 (m, 2H), 7.34-7.23 (m, 5H), 6.91 (dd,, J=2.22 Hz, J=8.46 Hz, 1H), 6.79 (d, J=2.22 Hz, 1H), 4.79 (s, 2H), 3.83 (s, 2H), 1.87-1.83 (m, 2H), 1.74-1.65 (m, 2H), 1.57-1.34 (m, 5H), 1.19-1.07 (m, 1H).

^{13}C NMR (100 MHz, DMSO-d6): δ 22.13, 24.04, 33.11, 44.01, 56.07, 94.20, 111.38, 113.14, 116.60, 117.60, 120.75, 121.76, 127.24, 128.81, 129.88, 130.08, 131.45, 135.61, 139.26, 153.19, 155.45, 160.20, 160.90.

ES+ $[M+H]^{+}$; m/z 495.2.

*(3-benzyl-4-oxo-spiro[1,3-benzoxazine-2,4'-tetrahydropyran]-7-yl) 3-nitrobenzenesulfonate (**7c1**)*

Product (**7c1**) was obtained from product (**6c**) by following a similar procedure to that described for product (**7b8**), using (3-nitro)-benzene-sulfonyl chloride instead of *p*-methoxybenzene-sulfonyl chloride, as yellow oil (15.6 mg, yield 55%)..

LC-UV purity: 99% (λ= 220 nm), 99% (λ= 254 nm).

^{1}H NMR (400 MHz, DMSO-d6): δ 8.68-8.65 (m, 1H), 8.51 (t, J=1.93 Hz, 1H), 8.29-8.26 (m, 1H), 7.98-7.89 (m, 2H), 7.36-7.24 (m, 5H), 7.01-6.98 (m, 2H), 4.82 (s, 2H), 3.68 (dd, J=11.42 Hz, J=4.64 Hz, 2H), 3.48 (t, J=11.42 Hz, 2H), 2.02-1.94 (m, 2H), 1.79 (d, J=13.40 Hz, 2H).

^{13}C NMR (100 MHz, DMSO-d6): δ 34.07, 44.21, 63.33, 91.82, 112.08, 117.05, 121.84, 123.47, 123.56, 127.39, 128.92, 129.07, 130.03, 130.61, 132.44, 134.68, 135.40, 148.82, 152.74, 155.10, 160.56.

ES+ $[M+Na]^{+}$; m/z 533.1.

*(3-benzyl-4-oxo-spiro[1,3-benzoxazine-2,4'-tetrahydropyran]-7-yl) 2,3-dihydro-1,4-benzodioxine-6-sulfonate (**7c2**)*

933 Product (**7c2**) was obtained from product (**6c**) by following a similar procedure to that described for
934 product (**7b8**), using 1,4-benzodioxan-6-sulfonyl chloride instead of *p*-methoxybenzene-sulfonyl
935 chloride, as white solid (17.0 mg, yield 61%)..
936 LC-UV purity: 99% (λ= 220 nm), 99% (λ= 254 nm).
937 ^{1}H NMR (400 MHz, DMSO-d6): δ 7.90-7.87 (m, 1H), 7.36-7.27 (m, 7H), 7.10 (d, J=8.54 Hz, 1H),
938 6.93-6.90 (m, 2H), 4.82 (s, 2H), 4.38-4.31 (m, 4H), 3.70 (dd, J=11.37 Hz, 4.65 Hz, 2H), 3.52 (t,
939 J=11.37 Hz, 2H), 2.02-1.94 (m, 2H), 1.80 (d, J=13.28 Hz, 2H).
940 ^{13}C NMR (100 MHz, DMSO-d6): δ 34.01, 44.17, 63.31, 64.49, 65.22, 91.11, 107.92, 11.71, 116.99,
941 117.48, 118.54, 122.57, 127.35, 129.02, 129.95, 130.25, 138.99, 143.92, 144.26, 149.94, 153.49,
942 154.75, 160.91.
943 ES+ $[M+Na]^{+}$; m/z 546.2.
944 *(3-benzyl-4-oxo-spiro[1,3-benzoxazine-2,4'-tetrahydropyran]-7-yl) 4-nitrobenzenesulfonate (**7c3**)*
945 Product (**7c3**) was obtained from product (**6c**) by following a similar procedure to that described for
946 product (**7b8**), using (4-nitro)-benzene-sulfonyl chloride instead of *p*-methoxybenzene-sulfonyl
947 chloride, as beige solid (11.6 mg, yield 49%).).
948 LC-UV purity: 99% (λ= 220 nm), 99% (λ= 254 nm).
949 ^{1}H NMR (400 MHz, DMSO-d6): δ 8.48-8.44 (m, 2H), 8.20-8.16 (m, 2H), 7.90 (d, J=8.50 Hz, 1H),
950 7.36-7.24 (m, 5H), 6.99 (d, J=2.28 Hz, 1H), 6.94 (dd, J=8.50 Hz, J=2.28 Hz, 1H), 4.82 (s, 2H), 3.68
951 (dd, J=11.40 Hz, J=4.72 Hz, 2H), 3.50 (t, J=11.40 Hz, 2H), 2.02-1.94 (m, 2H), 1.81 (d, J=13.25 Hz,
952 2H).
953 ^{13}C NMR (100 MHz, DMSO-d6): δ 160.56, 155.11, 153.00, 151.66, 139.34, 138.99, 131.90,
954 130.69, 130.27, 129.02, 127.53, 127.42, 125.55, 117.77, 116.98, 111.85, 91.20, 63.27, 43.96, 34.13.
955 ES+ $[M+H]^{+}$; m/z 511.1.
956
957 **[^{3}H]CP 55,940 Displacement Assay.** The binding affinity of synthesized compounds towards CB_2
958 was determined by [^{3}H]CP 55,940 displacement assays, performed through a standardized high-

959 throughput CB_2 binding procedure, as previously described [62]. Membrane fractions (2.5 μg) of
960 Chinese hamster ovary (CHO) cells stably overexpressing human CB_2 (Millipore Sigma,
961 Burlington, MA USA cod. HTS020M) were incubated in 50 mM Tris-HCl, 5 mM $MgCl_2$, 1 mM
962 $CaCl_2$, 2 mg/mL BSA, pH 7.4 (final volume: 200 μL) for 30 minutes at 37 °C, in the presence of 0.8
963 nM [^{3}H]CP 55,940 (164.9 Ci/mmol; PerkinElmer Life Sciences, Boston, MA, USA), with or
964 without test compounds. Non-specific binding was determined in the presence of 1 μM unlabelled
965 CP 55,940 (Cayman Chemical Company, Ann Arbor, MI, USA). Both 0.1 μM SR144528 (Cayman
966 Chemical) and 0.1 μM JWH-015 (Cayman Chemicals) were used as positive controls, and 0.1 μM
967 SR141617A (Cayman Chemicals) was used as negative control. The assay was stopped by three
968 washes with ice-cold washing buffer (50 mM Tris-HCl, 500 mM $NaCl_2$, 1 mg/mL BSA, pH 7.4),
969 followed by rapid filtration through glass fiber filters (Whatman GF/B) presoaked for 30 minutes
970 with 0.25% polyethylenimine (PEI), and radioactivity was read by scintillation β-Counter (Perkin
971 Elmer Life Science). Displacement of tritiated CP55,940 was initially assessed by using test
972 molecules at the final concentration of 0.1 μM and those showing percentage displacement of at
973 least 20% were further tested for their functional activity as follows. Each condition in the assays
974 was repeated in quintuplicate, in at least three independent experiments.

975 **[^{35}S]GTPγS Assay.** Functional activity and selectivity (towards CB_2 over CB_1) of the ligands were
976 evaluated by [^{35}S]GTPγS assay through rapid filtration assay, as described [85] and with slight
977 modifications [62]. Briefly, 5 μg ChemiSCREEN™ CB_2 Membrane Preparation (Millipore Sigma
978 cod. HTS020M2) were permeabilized by addition of an equal mass of saponin and pre-incubated
979 for 20 minutes at room temperature with compounds in a non-binding 96-well plate, containing
980 assay buffer (20 mM HEPES, 100 mM NaCl, 10 mM $MgCl_2$, pH 7.4 plus 10 μM GDP); then,
981 samples were incubated with 0.3 nM [^{35}S]GTPγS (1250 Ci/mmol, Perkin Elmer) for 30 minutes at
982 37 °C. Assay was stopped by adding ice-cold 100 mM sodium phosphate buffer (pH 7.4) and
983 followed by rapid filtration through glass fiber filters (Whatman GF/B) presoaked for 30 minutes

with 0.25% PEI; residual radioactivity was read by scintillation β-Counter. In order to distinguish agonist from antagonist and inverse agonist ligands, in a first set of experiments, CB_2 ligands were tested at 10 μM and 100 μM, in the presence or in the absence of 30 nM CP 55,940; compounds showing agonistic activity towards CB_2 were further tested at increasing concentrations (0-100 μM) by employing ChemiSCREEN™ CB_2 Membrane Preparation, as above described, or ChemiSCREEN™ CB_1 Membrane Preparation (10 μg/well Millipore Sigma, cod. HTS019M). Basal levels of [^{35}S]GTP binding were measured in untreated membrane samples and non-specific binding was determined in the absence of receptor ligands and in the presence of 0.1 μM "cold" GTP. 1 μM JHW-015 and 1 μM ACEA (Cayman Chemicals) were used as reference agonists for CB_2 and CB_1, respectively. Each condition in the assays was repeated in quintuplicate, in at least three independent experiments. pEC_{50} values were determined for each compound by non-linear curve fitting, using GraphPad Prism software (version 9.4.1. for Windows).

Cell Culture. Human triple-negative BT549 (ATCC HTB-122), MDA-MB-231 (ATCC HTB-26) and HER2-positive HCC1954 (ATCC CRL-2339) breast cancer cells were maintained in RPMI-1640 culture medium, supplemented with 0.023 U/mL insulin, 0.1 mg/mL sodium pyruvate, 100 μg/mL kanamycin and 10% foetal bovine serum. Human epithelial breast MCF10A cells (ATCC CRL-10317), a widely recognized *in vitro* model of normal breast cells[86], were grown in Dulbecco's modified Eagle's medium (DMEM)/F-12 medium (1:1, v/v) supplemented with 0.5 μg/mL hydrocortisone, 10 μg/mL insulin, 20 ng/mL EGF, 0.1 μg/mL cholera toxin, 100 U/mL penicillin, 100 U/mL streptomycin and 5% horse serum. Cell lines were grown in a humidified 5% CO_2 atmosphere at 37 °C and regularly tested for the absence of mycoplasma, by using either MycoStrip™ - Mycoplasma Detection Kit (InvivoGen, Toulouse, France) or LookOut® Mycoplasma qPCR Detection Kit (Sigma Aldrich, Sant Luis, Mo).

MTT Assay. Breast cancer and not-tumorigenic epithelial breast cells were seeded onto 96-well plates at a density of 1.5 x 10^4 cells/well and incubated on. The day after, sub-confluent cells were

1009 treated with test compound at 37 °C at the indicated concentrations and for the indicated time
1010 periods. Cell viability was evaluated via 3-(4,5-dimethylthiazol-2-yl)-2,5-diphenyl tetrazolium
1011 bromide (MTT) assay. Briefly, after treatments, culture medium was removed, MTT reagent (Sigma
1012 Aldrich) was added to each well (final concentration: 1 mg/mL) and cells were incubated at 37°C
1013 for 3 hours in the dark; formazan crystals were then dissolved in DMSO and color development was
1014 monitored at 590 nm in a multiwell scanning spectrophotometer (BS1000 Spectra count, Packard
1015 BioScience Co., Meridien, CT).
1016 **Transfection.** For *CNR2* gene silencing, BT549 cells were transfected with 50 nM *CNR2* siRNA
1017 (Hs_CNR2_1 FlexiTube siRNA SI00029064; Qiagen, Germantown, MD, USA) or scramble
1018 negative control (cod. 1027281, Qiagen), by using Lipofectamine RNAiMAX (Invitrogen,
1019 Heidelberg, Germany), according to manufacturer's instructions. After 24 hours, cells were treated
1020 with 10 μM **7b5** for further 24 hours, before evaluating proliferation as above reported.
1021 **Western Blotting.** Protein samples (20-40 μg/lane) from whole lysates were subjected to SDS-
1022 PAGE under reducing conditions, electroblotted onto PVDF membranes, incubated with specific
1023 antibodies and detected with enhanced chemiluminescence kit (Santa Cruz Biotechnology, Santa
1024 Cruz, CA, USA). The specific primary antibodies used were anti-CB_2 (1:500, cod. 101550, Cayman
1025 Chemicals), anti-ERK 1/2 (1:1000, cod. 4695, Cell Signaling Technology, Danvers, MA), anti-p-
1026 ERK 1/2 (1:100 cod. sc-7383, Santa Cruz Biotechnology) and anti-β-tubulin (1:500, sc-166729,
1027 Santa Cruz Biotechnology).
1028 **Colony Forming Unit (CFU) Assay.** BT549 cells were seeded in 6-well plates at a density of 1 x
1029 10^3 cells/well and grown at 37 °C for at least 14 days, in the presence of either vehicle or 10 μM
1030 **7b5**. Afterwards, colonies were fixed and stained with 6% glutaraldehyde and 0.5% crystal violet
1031 solution, for 30 minutes. After washes with distilled water, number of colonies was counted using
1032 an inverted phase contrast microscope (Zeiss; 10 X objective) as reported [87].
1033 **Pro-inflammatory cytokine quantification.** BT549 cells were seeded onto 96-well plates at a
1034 density of 1.5 x 10^4 cells/well and after 24 hours, sub-confluent cells were treated with vehicle or 10

μM **7b5**, at 37 °C for 48 hours. Culture supernatants (50 μl) were collected and TNF-α and IL-6 amounts were measured, respectively, through the TNF alpha Human ELISA Kit and IL-6 Human ELISA Kit (Thermo Fisher Scientific Inc. Rockford, IL), according to the manufacturer instructions. The absorbance values at 450 nm of unknown samples were always within the linearity range of calibration curves drawn with increasing concentration of recombinant cytokine (0-1000 pg/mL).

Statistical Analysis. Data are expressed as the mean ± SEM of at least three experiments. Statistical evaluation was performed using one-way analysis of variance (ANOVA), followed by Bonferroni t test. Differences were considered statistically significant at $p < 0.05$.

Selection and Refinement of CB_2 Structure. For docking and MD studies, we selected the crystal structure of CB_2 in complex with the agonist AM12033 (PDB code: 6KPC) [80], given the similarity between the latter and our newly synthesized **7b5** ligand. Since this structure missed ICL3 (*i.e.,* the third intercellular loop), the cryo-EM structure of agonist-bound CB_2 in complex with a G_i protein (PDB code: 6PT0) [81] was used as template for its reconstruction, considering that the latter structure was the only one with the solved ICL3 loop. Residues $V220^{5.69}$ to $S222^{5.71}$ of helix 5 and residues $R238^{6.28}$ to $V253^{6.43}$ of helix 6 were also involved in the modeling stage since the conformation of these regions resulted dissimilar between the two CB_2 crystal structures. The entire procedure was carried out by using the Refine Loops module available in Prime with default settings [88]. Finally, the protein preparation wizard tool [89,90] implemented in the Schrödinger suite was employed to carry out energy minimization on the chimeric protein structure, to remove nonstructural water molecules and assign protonation and tautomeric states of Asp, Arg, Glu, His and Lys residues at physiological pH. The Ballesteros-Weinstein numbering scheme [91] was adopted to identify the CB_2 residues. For the sake of completeness, being $C162^{45.50}$ the most conserved ECL2 (the second extracellular loop) residue among Class A GPCRs, we referred to $F183^{ECL2}$ as $F183^{45.54}$.

Molecular Docking. The tridimensional structure of **7b5** was built with the 2D-sketcher tool of the Schrödinger suite. Then, it was treated with the ligprep tool [92] to evaluate all the possible tautomers

and protonation states at physiological pH. A grid box centered on the center of mass of the AM12033 co-crystallized ligand, with a volume of 10 Å × 10 Å × 10 Å and 25 Å × 25 Å × 25 Å for inner and outer boxes, respectively, was computed by using the Receptor Grid Generation panel. For the simulations, the Extra Precision (XP) docking mode [79] was employed. This protocol was validated by redocking AM12033 co-crystallized ligand whose best pose returned a Root Mean Square Deviation (RMSD), based on heavy atoms only, as small as 0.844 Å.

Molecular Dynamics. As first step, the receptor N- and C- terminal residues were capped with acetyl and *N*-methyl groups, respectively, by employing the Protein Preparation Wizard tool implemented in the Schrödinger package. The system formed by the CB_2-**7b5** complex was inserted in a 95 Å × 95 Å (along x and y axes) pre-equilibrated box formed by a 1-palmitoyl-2-oleoylphosphatidylcholine (POPC)—cholesterol (7:3 molar ratio) bilayer and solvated with a 18 Å (along z) water layer using the TIP3P model. The membrane-builder tool of CHARMM-GUI.org (http://www.charmm-gui.org) was employed for these purposes.[93,94] The protein and lipids were parameterized by using the *ff14SB* and *lipid17* Amber force field, respectively. Atomic partial charges of the ligand were computed by using a two-steps restrained electrostatic potential (RESP) fitting procedure. The Gaussian16 software [95] was initially used to optimize the ligand geometry and to compute the electrostatic potential (ESP) using the 6-31G* basis set at the Hartree-Fock level of theory. The ESP was then fitted into atomic partial charges thanks to the two-stages restrained electrostatic potential (RESP) [96] fitting procedure implemented in Antechamber [97] The topology files were prepared with the *tleap* module of AmberTools20 and then converted into GROMACS format by means of ParmEd. All MD simulations were performed by employing the GROMACS 2020.6 software [82]. The cutoff employed for the computation of the short-rage interactions was of 12 Å, whereas the Particle Mesh Ewald [98] method (with a 1.0 Å grid spacing in periodic boundary conditions) was used for the treatment of long-range ones. A 2 fs integration time step was allowed by constraining bonds with the non-iterative LINCS algorithm [99]. The system was equilibrated according to the following protocol. In order to remove all the steric clashes, three runs of energy

1087 minimization were performed following three different phases: first, only hydrogen atoms were
1088 minimized, and all heavy atoms were kept fixed; in the second step, the lipid bilayer was also
1089 relaxed; and in the last step all the atoms were minimized. Then, the complex was equilibrated and
1090 heated up to 300 K, alternating NPT and NVT cycles (for a total of 30 ns) with the Berendsen
1091 coupling bath and barostat, while applying gradually decreasing harmonic constraints on the heavy
1092 atoms of the membrane, protein, and ligand. Eventually, 3 μs production run was performed with
1093 the leap-frog integrator in the NPT ensemble; the pressure of 1 atm and the temperature of 300 K
1094 were kept constant with the stochastic velocity rescaling [100] and Parrinello-Rahman [101] algorithms,
1095 respectively.

1096 The ligand behavior within the CB_2 binding site was monitored by computing RMSD values on the
1097 heavy atoms and the contacts established with surrounding amino acids throughout the trajectory.
1098 The overall stability of CB_2 was inspected by calculating the RMSD values of C_α of all the helices
1099 (Figure S10 of the Supporting Information). For sake of completeness, for the RMSD calculation,
1100 all frames were aligned to the latter atoms.

1101 **CB_1 Homology Modeling**. A "dynamic" homology model of the CB_1 was constructed by using as
1102 template the relaxed average structure of CB_2 taken from MD simulation, since it was not possible
1103 to correctly superimpose the CB_1 crystal structure with the latter. Such a procedure was
1104 implemented with the aim of highlighting even small variations concerning the side chain
1105 conformations within the orthosteric sites of the two isoforms. The fasta sequence of human CB_1
1106 was retrieved from the Universal Protein resource (UniProt) [102] with entry P21554. The model was
1107 built by using Prime [88]. As a first step, CB_1 and CB_2 sequences were aligned using the Jalview
1108 software [103] showing a value of identity equal to 32% . The target and template structures were then
1109 aligned by employing the ClustalW method implemented in Prime and the CB_1 secondary structure
1110 was predicted with the SSPro interface. Finally, ECL2 residues from $E164^{45.44}$ to $V169^{45.49}$ of the
1111 CB_1 constructed model were refined by using the Refined Loop package, since this loop differed in

length from that of CB_2. For completeness, the ligand present in the template structure was included during the homology modeling.

ASSOCIATED CONTENT

Supporting Information

Figure S1. Distribution of MW in ChEMBL 31. Figure S2. Distribution of logP in ChEMBL 31. Figure S3. Log concentration-response curves for **7b5** effects on stimulation of [35S]GTPγS binding in CB2 membrane preparation. Figure S4. Anti-proliferative effects of **7b5** on different breast cell lines. Figure S5. Anti-proliferative effects of JWH-015 on BT549 breast cancer cells. Figure S6. Western blot analysis of CB_2 expression in BT549 cells transfected with either *CNR2* siRNA or with scramble oligo for 24 hours. Figure S7. Plots of the distances between: a) $F94^{2.64}$ and 7b5 benzyl ring; b) $F183^{45.54}$ and the **7b5** benzoxazine core; c) $F87^{2.57}$ and 7b5 benzoxazine core; and d) $W194^{5.43}$ and **7b5** thienyl moiety. Figure S8. $R131^{3.50}$-$D240^{6.30}$ distance plot throughout the MD trajectory. Figure S9. Molecular docking analysis performed on compounds **7a3** and **7b9.** Figure S10. RMSD plots of helices TM1 to TM7 throughout the MD trajectory. Table S1. Structure of **5a**-**5b** intermediates. Table S2. Structure of **6b** and **6c** intermediates. Table S3. Structures of the 25 2,3-dihydro-4H-benzo[e][1,3]oxazin-4-one derivatives. Analytical Data including ^{1}H-NMR, ^{13}C-NMR, MS and HPLC. File_S1.csv reports details about the 115 targets taken from ChEMBL (release 31). CB2_docking_complex_no-hydrogen.pdb reports the docking based ligand bound CB2 complex. CB2_MD_complex_no-hydrogen.pdb reports the MD based ligand bound CB2 complex. CB1_Dynamic-homology_model.pdb reports the homology model derived from MD on the ligand bound CB2 complex.

AUTHOR INFORMATION

Corresponding Author

* Alessandra Topai − C4T S.r.l Colosseum Combinatorial Chemistry Centre for Technology, Via della Ricerca Scientifica snc, 00133, Rome, Italy; https://orcid.org/0000-0002-0698-9900; Phone: 0039 0672594030; Email: alessandra.topai@c4t.it.

* Orazio Nicolotti − Department of Pharmacy-Pharmaceutical Sciences, University of the Studies of Bari "Aldo Moro", Via E. Orabona 4, 70125, Bari, Italy; https://orcid.org/0000-0001-6533-5539; Phone: 0039 0805442551; Email: orazio.nicolotti@uniba.it.

* Mauro Maccarrone − Department of Biotechnological and Applied Clinical Sciences, University of L'Aquila, Via Vetoio, 67100, Coppito, L'Aquila, Italy; https://orcid.org/0000-0002-3990-2963; Phone: 0039 0862433547; Email: mauro.maccarrone@univaq.it.

Authors

Nicola Gambacorta −Department of Pharmacy-Pharmaceutical Sciences, University of the Studies of Bari "Aldo Moro", Via E.Orabona 4, 70125, Bari, Italy; https://orcid.org/0000-0003-1965-1519.

Valeria Gasperi − Department of Experimental Medicine, Tor Vergata University of Rome, Via Montpellier 1, 00133, Rome, Italy; https://orcid.org/0000-0003-3200-8093.

Tatiana Guzzo − C4T S.r.l Colosseum Combinatorial Chemistry Centre for Technology, Via della Ricerca Scientifica snc, 00133, Rome, Italy; https://orcid.org/0000-0002-3696-8502.

Francesco Saverio Di Leva − Department of Pharmacy, University of Naples Federico II, 80131 Via D. Montesano 49, 80131, Naples, Italy; https://orcid.org/0000-0002-2294-0656.b

Fulvio Ciriaco − Department of Chemistry, University of the Studies of Bari "Aldo Moro", via E. Orabona 4, 70125, Bari, Italy; https://orcid.org/0000-0002-0695-6607.

Cristina Sánchez − Department of Biochemistry and Molecular Biology, School of Biology, Complutense University, C/ José Antonio Nováis, 12, 28040, Madrid, Spain; https://orcid.org/0000-0002-1428-3078.

Valentina Tullio - Department of Experimental Medicine, Tor Vergata University of Rome, Via Montpellier 1, 00133, Rome, Italy; https://orcid.org/0000-0002-4109-1805.

Diego Rozzi − C4T S.r.l Colosseum Combinatorial Chemistry Centre for Technology, Via della Ricerca Scientifica snc, 00133, Rome, Italy; https://orcid.org/0000-0002-3696-8502.

Luciana Marinelli − Department of Pharmacy, University of Naples Federico II, 80131 Via D. Montesano 49, 80131, Naples, Italy; https://orcid.org/0000-0002-4084-8044.

Author Contributions

The manuscript was written through contributions of all authors. All authors have given approval to the final version of the manuscript. # N.G., V.G. and T.G. contributed equally.

Funding Sources

NG, FC and ON gratefully thank Horizon Europe Seeds "L'intelligenza artificiale a tutela della salute in età pediatrica. Implementazione di una piattaforma digitale per il design di farmaci pediatrici sicuri", Università degli Studi di Bari (Bari, Italy) (CUP: H99J21017390006). MM gratefully acknowledges the Italian Ministry of University and Research (MUR) for financial support under the competitive grant PRIN 2017-2017BTHJ4R, and the Department of Biotechnological and Applied Clinical Sciences - University of L'Aquila for the intramural competitive grant DISCAB GRANT 07_DG_2022_12. Part of this work was financed by Regione Lazio – DTB – Fondi CIPE (NUMORECA PROJECT).

Notes

The authors declare no competing financial interest.

ABBREVIATIONS

ANOVA, analysis of variance; CB_1, cannabinoid receptor 1; CB_2, cannabinoid receptor 2; CFU, colony forming unit; CHO, chinese hamster ovary; CNS, central nervous system; Δ^9-THC, Δ^9-tetrahydrocannabinol; DMF *N,N*-dimethylformamide; DMSO-d6, deuterated dimethyl sulfoxide; DMEM, Dulbecco's modified Eagle's medium; EC_{50}, maximal effective concentration; ECL2,

second extracellular loop; ECS, endocannabinoid system; ESP, electrostatic potential; ERK, extracellular signal-regulated kinase; interleukin-6, IL-6; J, coupling constant; MD, molecular dynamics; MHz, megahertz; MOM, methoxymethyl; MTT, (3-[4,5-dimethylthiazol-2-yl]-2,5 diphenyl tetrazolium bromide); mmol, millimole; µL, microliter; µM, micromolar; NMR, nuclear magnetic resonance; nM, nanomolar; on, over night; PDB, code protein data bank; PEI, polyethylenimine; pg, picograms; rt, room temperature; RESP, restrained electrostatic potential; RMSD, root-mean-square deviation of atomic positions; RP, reverse phase; rt, room temperature; SAR, structure activity relationship; ppm, parts per million; SEM, standard error of mean; SMILE, simplified molecular input line entry system; TMS, tetramethylsilane; TNF-α, tumor necrosis factor; UniProt, Universal Protein resource; XP, extra precision.

REFERENCES

(1) Munro, S.; Thomas, K. L.; Abu-Shaar, M. Molecular Characterization of a Peripheral Receptor for Cannabinoids. *Nature* **1993**, *365* (6441), 61–65. https://doi.org/10.1038/365061a0.

(2) Gasperi, V.; Guzzo, T.; Topai, A.; Gambacorta, N.; Ciriaco, F.; Nicolotti, O.; Maccarrone, M. Recent Advances on Type-2 Cannabinoid (CB2) Receptor Agonists and Their Therapeutic Potential. *Current Medicinal Chemistry* **2022**. https://doi.org/10.2174/0929867329666220825161603.

(3) Devane, W. A.; Dysarz, F. A.; Johnson, M. R.; Melvin, L. S.; Howlett, A. C. Determination and Characterization of a Cannabinoid Receptor in Rat Brain. *Molecular Pharmacology* **1988**, *34* (5), 605–613.

(4) Gaoni, Y.; Mechoulam, R. Isolation, Structure, and Partial Synthesis of an Active Constituent of Hashish. *Journal of the American Chemical Society* **1964**, *86* (8), 1646–1647. https://doi.org/10.1021/ja01062a046.

(5) Durieux, L. J. A.; Gilissen, S. R. J.; Arckens, L. Endocannabinoids and Cortical Plasticity: CB1R as a Possible Regulator of the Excitation/Inhibition Balance in Health and Disease. *European Journal of Neuroscience* **2022**, *55* (4), 971–988. https://doi.org/10.1111/ejn.15110.

(6) Kendall, D. A.; Yudowski, G. A. Cannabinoid Receptors in the Central Nervous System: Their Signaling and Roles in Disease. *Frontiers in Cellular Neuroscience* **2017**, *10*.

(7) O'Sullivan, S. E.; Yates, A. S.; Porter, R. K. The Peripheral Cannabinoid Receptor Type 1 (CB1) as a Molecular Target for Modulating Body Weight in Man. *Molecules* **2021**, *26* (20), 6178. https://doi.org/10.3390/molecules26206178.

(8) El-Atawneh, S.; Hirsch, S.; Hadar, R.; Tam, J.; Goldblum, A. Prediction and Experimental Confirmation of Novel Peripheral Cannabinoid-1 Receptor Antagonists. *Journal of Chemical Information and Modeling* **2019**, *59* (9), 3996–4006. https://doi.org/10.1021/acs.jcim.9b00577.

(9) Pi-Sunyer, F. X.; Aronne, L. J.; Heshmati, H. M.; Devin, J.; Rosenstock, J.; RIO-North America Study Group, for the. Effect of Rimonabant, a Cannabinoid-1 Receptor Blocker, on Weight and Cardiometabolic Risk Factors in Overweight or Obese PatientsRIO-North America: A Randomized Controlled Trial. *JAMA* **2006**, *295* (7), 761–775. https://doi.org/10.1001/jama.295.7.761.

(10) Simard, M.; Rakotoarivelo, V.; Di Marzo, V.; Flamand, N. Expression and Functions of the CB2 Receptor in Human Leukocytes. *Frontiers in Pharmacology* **2022**, *13*.

(11) Rajesh, M.; Mukhopadhyay, P.; Bátkai, S.; Arif, M.; Varga, Z. V.; Mátyás, C.; Paloczi, J.; Lehocki, A.; Haskó, G.; Pacher, P. Correction to: Cannabinoid Receptor 2 Activation Alleviates Diabetes-Induced Cardiac Dysfunction, Inflammation, Oxidative Stress, and Fibrosis. *Geroscience* **2022**, *44* (3), 1743–1745. https://doi.org/10.1007/s11357-022-00593-5.

(12) Wright, K. L.; Duncan, M.; Sharkey, K. A. Cannabinoid CB2 Receptors in the Gastrointestinal Tract: A Regulatory System in States of Inflammation. *British Journal of Pharmacology* **2008**, *153* (2), 263–270. https://doi.org/10.1038/sj.bjp.0707486.

(13) Gasperi, V.; Evangelista, D.; Chiurchiù, V.; Florenzano, F.; Savini, I.; Oddi, S.; Avigliano, L.; Catani, M. V.; Maccarrone, M. 2-Arachidonoylglycerol Modulates Human Endothelial Cell/Leukocyte Interactions by Controlling Selectin Expression through CB1 and CB2 Receptors. *The International Journal of Biochemistry & Cell Biology* **2014**, *51*, 79–88. https://doi.org/10.1016/j.biocel.2014.03.028.

(14) Jenkin, K. A.; McAinch, A. J.; Briffa, J. F.; Zhang, Y.; Kelly, D. J.; Pollock, C. A.; Poronnik, P.; Hryciw, D. H. Cannabinoid Receptor 2 Expression in Human Proximal Tubule Cells Is Regulated by Albumin Independent of ERK1/2 Signaling. *CPB* **2013**, *32* (5), 1309–1319. https://doi.org/10.1159/000354529.

(15) Notarnicola, M.; Tutino, V.; Tafaro, A.; Bianco, G.; Guglielmi, E.; Caruso, M. G. Dietary Olive Oil Induces Cannabinoid CB2 Receptor Expression in Adipose Tissue Of Apc Min/+ Transgenic Mice. *Nutrition and Healthy Aging* **2016**, *4* (1), 73–80. https://doi.org/10.3233/NHA-160008.
(16) Lin, X.; Xu, Z.; Carey, L.; Romero, J.; Makriyannis, A.; Hillard, C. J.; Ruggiero, E.; Dockum, M.; Houk, G.; Mackie, K.; Albrecht, P. J.; Rice, F. L.; Hohmann, A. G. A Peripheral CB2 Cannabinoid Receptor Mechanism Suppresses Chemotherapy-Induced Peripheral Neuropathy: Evidence from a CB2 Reporter Mouse. *Pain* **2022**, *163* (5), 834–851. https://doi.org/10.1097/j.pain.0000000000002502.
(17) Rossi, F.; Tortora, C.; Punzo, F.; Bellini, G.; Argenziano, M.; Di Paola, A.; Torella, M.; Perrotta, S. The Endocannabinoid/Endovanilloid System in Bone: From Osteoporosis to Osteosarcoma. *International Journal of Molecular Sciences* **2019**, *20* (8), 1919. https://doi.org/10.3390/ijms20081919.
(18) Cassano, T.; Calcagnini, S.; Pace, L.; De Marco, F.; Romano, A.; Gaetani, S. Cannabinoid Receptor 2 Signaling in Neurodegenerative Disorders: From Pathogenesis to a Promising Therapeutic Target. *Frontiers in Neuroscience* **2017**, *11*.
(19) Onaivi, E. S. Neuropsychobiological Evidence for the Functional Presence and Expression of Cannabinoid CB2 Receptors in the Brain. *NPS* **2006**, *54* (4), 231–246. https://doi.org/10.1159/000100778.
(20) Kim, J.; Li, Y. Chronic Activation of CB2 Cannabinoid Receptors in the Hippocampus Increases Excitatory Synaptic Transmission. *The Journal of Physiology* **2015**, *593* (4), 871–886. https://doi.org/10.1113/jphysiol.2014.286633.
(21) Stempel, A. V.; Stumpf, A.; Zhang, H.-Y.; Özdoğan, T.; Pannasch, U.; Theis, A.-K.; Otte, D.-M.; Wojtalla, A.; Rácz, I.; Ponomarenko, A.; Xi, Z.-X.; Zimmer, A.; Schmitz, D. Cannabinoid Type 2 Receptors Mediate a Cell Type-Specific Plasticity in the Hippocampus. *Neuron* **2016**, *90* (4), 795–809. https://doi.org/10.1016/j.neuron.2016.03.034.
(22) Viscomi, M. T.; Oddi, S.; Latini, L.; Pasquariello, N.; Florenzano, F.; Bernardi, G.; Molinari, M.; Maccarrone, M. Selective CB2 Receptor Agonism Protects Central Neurons from Remote Axotomy-Induced Apoptosis through the PI3K/Akt Pathway. *Journal of Neuroscience* **2009**, *29* (14), 4564–4570. https://doi.org/10.1523/JNEUROSCI.0786-09.2009.
(23) Jones, I. A.; Togashi, R.; Wilson, M. L.; Heckmann, N.; Vangsness, C. T. Intra-Articular Treatment Options for Knee Osteoarthritis. *Nature Reviews Rheumatology* **2019**, *15* (2), 77–90. https://doi.org/10.1038/s41584-018-0123-4.
(24) Fedewa, M. V.; Bentley, J. L.; Higgins, S.; Kindler, J. M.; Esco, M. R.; MacDonald, H. V. Celiac Disease and Bone Health in Children and Adolescents: A Systematic Review and Meta-Analysis. *Journal of Clinical Densitometry* **2020**, *23* (2), 200–211. https://doi.org/10.1016/j.jocd.2019.02.003.
(25) Sophocleous, A.; Marino, S.; Logan, J. G.; Mollat, P.; Ralston, S. H.; Idris, A. I. Bone Cell-Autonomous Contribution of Type 2 Cannabinoid Receptor to Breast Cancer-Induced Osteolysis *. *Journal of Biological Chemistry* **2015**, *290* (36), 22049–22060. https://doi.org/10.1074/jbc.M115.649608.
(26) Capozzi, A.; Mattei, V.; Martellucci, S.; Manganelli, V.; Saccomanni, G.; Garofalo, T.; Sorice, M.; Manera, C.; Misasi, R. Anti-Proliferative Properties and Proapoptotic Function of New CB2 Selective Cannabinoid Receptor Agonist in Jurkat Leukemia Cells. *International Journal of Molecular Sciences* **2018**, *19* (7), 1958. https://doi.org/10.3390/ijms19071958.
(27) Bettiga, A.; Aureli, M.; Colciago, G.; Murdica, V.; Moschini, M.; Lucianò, R.; Canals, D.; Hannun, Y.; Hedlund, P.; Lavorgna, G.; Colombo, R.; Bassi, R.; Samarani, M.; Montorsi, F.; Salonia, A.; Benigni, F. Bladder Cancer Cell Growth and Motility Implicate Cannabinoid 2 Receptor-Mediated Modifications of Sphingolipids Metabolism. *Scientific Reports* **2017**, *7* (1), 42157. https://doi.org/10.1038/srep42157.

(28) Pérez-Gómez, E.; Andradas, C.; Blasco-Benito, S.; Caffarel, M. M.; García-Taboada, E.; Villa-Morales, M.; Moreno, E.; Hamann, S.; Martín-Villar, E.; Flores, J. M.; Wenners, A.; Alkatout, I.; Klapper, W.; Röcken, C.; Bronsert, P.; Stickeler, E.; Staebler, A.; Bauer, M.; Arnold, N.; Soriano, J.; Pérez-Martínez, M.; Megías, D.; Moreno-Bueno, G.; Ortega-Gutiérrez, S.; Artola, M.; Vázquez-Villa, H.; Quintanilla, M.; Fernández-Piqueras, J.; Canela, E. I.; McCormick, P. J.; Guzmán, M.; Sánchez, C. Role of Cannabinoid Receptor CB2 in HER2 Pro-Oncogenic Signaling in Breast Cancer. *JNCI: Journal of the National Cancer Institute* **2015**, *107* (6), djv077. https://doi.org/10.1093/jnci/djv077.

(29) Hanlon, K. E.; Lozano-Ondoua, A. N.; Umaretiya, P. J.; Symons-Liguori, A. M.; Chandramouli, A.; Moy, J. K.; Kwass, W. K.; Mantyh, P. W.; Nelson, M. A.; Vanderah, T. W. Modulation of Breast Cancer Cell Viability by a Cannabinoid Receptor 2 Agonist, JWH-015, Is Calcium Dependent. *Breast Cancer (Dove Med Press)* **2016**, *8*, 59–71. https://doi.org/10.2147/BCTT.S100393.

(30) Hernández, F.; Sánchez, A.; Rendón-Vallejo, P.; Millán-Pacheco, C.; Alcaraz, Y.; Delgado, F.; Vázquez, M. A.; Estrada-Soto, S. Synthesis, Ex Vivo and in Silico Studies of 3-Cyano-2-Pyridone Derivatives with Vasorelaxant Activity. *European Journal of Medicinal Chemistry* **2013**, *70*, 669–676. https://doi.org/10.1016/j.ejmech.2013.10.018.

(31) Mao, Y.; Huang, Y.; Zhang, Y.; Wang, C.; Wu, H.; Tian, X.; Liu, Y.; Hou, B.; Liang, Y.; Rong, H.; Gu, X.; Ma, Z. Cannabinoid Receptor 2-selective Agonist JWH015 Attenuates Bone Cancer Pain through the Amelioration of Impaired Autophagy Flux Induced by Inflammatory Mediators in the Spinal Cord. *Molecular Medicine Reports* **2019**, *20* (6), 5100–5110. https://doi.org/10.3892/mmr.2019.10772.

(32) Ehrhart, J.; Obregon, D.; Mori, T.; Hou, H.; Sun, N.; Bai, Y.; Klein, T.; Fernandez, F.; Tan, J.; Shytle, R. D. Stimulation of Cannabinoid Receptor 2 (CB2) Suppresses Microglial Activation. *Journal of Neuroinflammation* **2005**, *2* (1), 29. https://doi.org/10.1186/1742-2094-2-29.

(33) Zhao, J.; Wang, M.; Liu, W.; Ma, Z.; Wu, J. Activation of Cannabinoid Receptor 2 Protects Rat Hippocampal Neurons against Aβ-Induced Neuronal Toxicity. *Neuroscience Letters* **2020**, *735*, 135207. https://doi.org/10.1016/j.neulet.2020.135207.

(34) Martín-Moreno, A. M.; Brera, B.; Spuch, C.; Carro, E.; García-García, L.; Delgado, M.; Pozo, M. A.; Innamorato, N. G.; Cuadrado, A.; de Ceballos, M. L. Prolonged Oral Cannabinoid Administration Prevents Neuroinflammation, Lowers β-Amyloid Levels and Improves Cognitive Performance in Tg APP 2576 Mice. *Journal of Neuroinflammation* **2012**, *9* (1), 8. https://doi.org/10.1186/1742-2094-9-8.

(35) Li, C.; Shi, J.; Wang, B.; Li, J.; Jia, H. CB2 Cannabinoid Receptor Agonist Ameliorates Novel Object Recognition but Not Spatial Memory in Transgenic APP/PS1 Mice. *Neuroscience Letters* **2019**, *707*, 134286. https://doi.org/10.1016/j.neulet.2019.134286.

(36) Wang, L.; Shi, F.-X.; Xu, W.-Q.; Cao, Y.; Li, N.; Li, M.; Wang, Q.; Wang, J.-Z.; Tian, Q.; Yu, L.-K.; Zhou, X.-W. The Down-Expression of ACE and IDE Exacerbates Exogenous Amyloid-β Neurotoxicity in CB2R –/– Mice. *Journal of Alzheimer's Disease* **2018**, *64* (3), 957–971. https://doi.org/10.3233/JAD-180142.

(37) Gómez-Gálvez, Y.; Palomo-Garo, C.; Fernández-Ruiz, J.; García, C. Potential of the Cannabinoid CB(2) Receptor as a Pharmacological Target against Inflammation in Parkinson's Disease. *Progress in Neuro-Psychopharmacology & Biological Psychiatry* **2016**, *64*, 200–208. https://doi.org/10.1016/j.pnpbp.2015.03.017.

(38) He, X.; Yang, L.; Huang, R.; Lin, L.; Shen, Y.; Cheng, L.; Jin, L.; Wang, S.; Zhu, R. Activation of CB2R with AM1241 Ameliorates Neurodegeneration via the Xist/MiR-133b-3p/Pitx3 Axis. *Journal of Cellular Physiology* **2020**, *235* (9), 6032–6042. https://doi.org/10.1002/jcp.29530.

(39) Fu, W.; Taylor, B. K. Activation of Cannabinoid CB2 Receptors Reduces Hyperalgesia in an Experimental Autoimmune Encephalomyelitis Mouse Model of Multiple Sclerosis. *Neuroscience Letters* **2015**, *595*, 1–6. https://doi.org/10.1016/j.neulet.2015.04.002.

(40) Alberti, T. B.; Barbosa, W. L. R.; Vieira, J. L. F.; Raposo, N. R. B.; Dutra, R. C. (−)-β-Caryophyllene, a CB2 Receptor-Selective Phytocannabinoid, Suppresses Motor Paralysis and Neuroinflammation in a Murine Model of Multiple Sclerosis. *International Journal of Molecular Sciences* **2017**, *18* (4), 691. https://doi.org/10.3390/ijms18040691.
(41) Tiberi, M.; Evron, T.; Saracini, S.; Boffa, L.; Mercuri, N. B.; Chintalacharuvu, S. R.; Atamas, S. P.; Chiurchiù, V. Potent T Cell-Mediated Anti-Inflammatory Role of the Selective CB2 Agonist Lenabasum in Multiple Sclerosis. *Neuropathology and Applied Neurobiology* **2022**, *48* (2), e12768. https://doi.org/10.1111/nan.12768.
(42) Kim, K.; Moore, D. H.; Makriyannis, A.; Abood, M. E. AM1241, a Cannabinoid CB2 Receptor Selective Compound, Delays Disease Progression in a Mouse Model of Amyotrophic Lateral Sclerosis. *European Journal of Pharmacology* **2006**, *542* (1), 100–105. https://doi.org/10.1016/j.ejphar.2006.05.025.
(43) Espejo-Porras, F.; García-Toscano, L.; Rodríguez-Cueto, C.; Santos-García, I.; de Lago, E.; Fernandez-Ruiz, J. Targeting Glial Cannabinoid CB2 Receptors to Delay the Progression of the Pathological Phenotype in TDP-43 (A315T) Transgenic Mice, a Model of Amyotrophic Lateral Sclerosis. *British Journal of Pharmacology* **2019**, *176* (10), 1585–1600. https://doi.org/10.1111/bph.14216.
(44) Rodríguez-Cueto, C.; Gómez-Almería, M.; García Toscano, L.; Romero, J.; Hillard, C. J.; de Lago, E.; Fernández-Ruiz, J. Inactivation of the CB2 Receptor Accelerated the Neuropathological Deterioration in TDP-43 Transgenic Mice, a Model of Amyotrophic Lateral Sclerosis. *Brain Pathology* **2021**, *31* (6), e12972. https://doi.org/10.1111/bpa.12972.
(45) Ghosh, K.; Zhang, G.-F.; Chen, H.; Chen, S.-R.; Pan, H.-L. Cannabinoid CB2 Receptors Are Upregulated via Bivalent Histone Modifications and Control Primary Afferent Input to the Spinal Cord in Neuropathic Pain. *Journal of Biological Chemistry* **2022**, *298* (6), 101999. https://doi.org/10.1016/j.jbc.2022.101999.
(46) Hanuš, L.; Breuer, A.; Tchilibon, S.; Shiloah, S.; Goldenberg, D.; Horowitz, M.; Pertwee, R. G.; Ross, R. A.; Mechoulam, R.; Fride, E. HU-308: A Specific Agonist for CB2, a Peripheral Cannabinoid Receptor. *Proceedings of the National Academy of Sciences* **1999**, *96* (25), 14228–14233.
(47) Huffman, J. W.; Liddle, J.; Yu, S.; Aung, M. M.; Abood, M. E.; Wiley, J. L.; Martin, B. R. 3-(1′,1′-Dimethylbutyl)-1-Deoxy-Δ8-THC and Related Compounds: Synthesis of Selective Ligands for the CB2 Receptor. *Bioorganic & Medicinal Chemistry* **1999**, *7* (12), 2905–2914. https://doi.org/10.1016/S0968-0896(99)00219-9.
(48) Vann, R. E.; Cook, C. D.; Martin, B. R.; Wiley, J. L. Cannabimimetic Properties of Ajulemic Acid. *Journal of Pharmacology and Experimental Therapeutics* **2007**, *320* (2), 678–686. https://doi.org/10.1124/jpet.106.111625.
(49) Montecucco, F.; Burger, F.; Mach, F.; Steffens, S. CB2 Cannabinoid Receptor Agonist JWH-015 Modulates Human Monocyte Migration through Defined Intracellular Signaling Pathways. *American Journal of Physiology-Heart and Circulatory Physiology* **2008**, *294* (3), H1145–H1155. https://doi.org/10.1152/ajpheart.01328.2007.
(50) van der Stelt, M.; Cals, J.; Broeders-Josten, S.; Cottney, J.; van der Doelen, A. A.; Hermkens, M.; de Kimpe, V.; King, A.; Klomp, J.; Oosterom, J.; Pols-de Rooij, I.; de Roos, J.; van Tilborg, M.; Boyce, S.; Baker, J. Discovery and Optimization of 1-(4-(Pyridin-2-Yl)Benzyl)Imidazolidine-2,4-Dione Derivatives As a Novel Class of Selective Cannabinoid CB2 Receptor Agonists. *Journal of Medicinal Chemistry* **2011**, *54* (20), 7350–7362. https://doi.org/10.1021/jm200916p.
(51) Mukhopadhyay, P.; Baggelaar, M.; Erdelyi, K.; Cao, Z.; Cinar, R.; Fezza, F.; Ignatowska-Janlowska, B.; Wilkerson, J.; van Gils, N.; Hansen, T.; Ruben, M.; Soethoudt, M.; Heitman, L.; Kunos, G.; Maccarrone, M.; Lichtman, A.; Pacher, P.; Van der Stelt, M. The Novel, Orally Available and Peripherally Restricted Selective Cannabinoid CB2 Receptor Agonist LEI-101

Prevents Cisplatin-Induced Nephrotoxicity. *British Journal of Pharmacology* **2016**, *173* (3), 446–458. https://doi.org/10.1111/bph.13338.
(52) Li, X.; Chang, H.; Bouma, J.; de Paus, L. V.; Mukhopadhyay, P.; Paloczi, J.; Mustafa, M.; van der Horst, C.; Kumar, S. S.; Wu, L.; Yu, Y.; van den Berg, R. J. B. H. N.; Janssen, A. P. A.; Lichtman, A.; Liu, Z.-J.; Pacher, P.; van der Stelt, M.; Heitman, L. H.; Hua, T. Structural Basis of Selective Cannabinoid CB2 Receptor Activation. *Nature Communication* **2023**, *14* (1), 1447. https://doi.org/10.1038/s41467-023-37112-9.
(53) Odan, M.; Ishizuka, N.; Hiramatsu, Y.; Inagaki, M.; Hashizume, H.; Fujii, Y.; Mitsumori, S.; Morioka, Y.; Soga, M.; Deguchi, M.; Yasui, K.; Arimura, A. Discovery of S-777469: An Orally Available CB2 Agonist as an Antipruritic Agent. *Bioorganic & Medicinal Chemistry Letters* **2012**, *22* (8), 2803–2806. https://doi.org/10.1016/j.bmcl.2012.02.072.
(54) Tang, Z.; Tan, Y.; Chen, H.; Wan, Y. Benzoxazine: A Privileged Scaffold in Medicinal Chemistry. *Current Medicinal Chemistry* **2022**. https://doi.org/10.2174/0929867329666220705140846.
(55) Alberga, D.; Gambacorta, N.; Trisciuzzi, D.; Ciriaco, F.; Amoroso, N.; Nicolotti, O. De Novo Drug Design of Targeted Chemical Libraries Based on Artificial Intelligence and Pair-Based Multiobjective Optimization. *Journal of Chemical Information and Modeling* **2020**, *60* (10), 4582–4593. https://doi.org/10.1021/acs.jcim.0c00517.
(56) Nicolotti, O.; Giangreco, I.; Introcaso, A.; Leonetti, F.; Stefanachi, A.; Carotti, A. Strategies of Multi-Objective Optimization in Drug Discovery and Development. *Expert Opinion on Drug Discovery* **2011**, *6* (9), 871–884. https://doi.org/10.1517/17460441.2011.588696.
(57) Su, Z.; Chai, H.; Xu, J.; Li, J. ZnCl 2 -Promoted Domino Reaction of 2-Hydroxybenzonitriles with Ketones for Synthesis of 1,3-Benzoxazin-4-Ones. *RSC Advances* **2021**, *11* (48), 29906–29911. https://doi.org/10.1039/D1RA04194K.
(58) Alessandra Topai,Teresa Fabiola Miscioscia, Fabio Barile, Tatiana Guzzo,Franco Minissi, Manolo Sablone, Mauro Maccarrone. Compounds of 2,3–Dihydro–4h-1,3–Benzoxazine–4–One, Method for Preparing Them and Pharmaceutical Form Comprising Them. WO2014097188A1, 2014.
(59) Mendez, D.; Gaulton, A.; Bento, A. P.; Chambers, J.; De Veij, M.; Félix, E.; Magariños, M. P.; Mosquera, J. F.; Mutowo, P.; Nowotka, M.; Gordillo-Marañón, M.; Hunter, F.; Junco, L.; Mugumbate, G.; Rodriguez-Lopez, M.; Atkinson, F.; Bosc, N.; Radoux, C. J.; Segura-Cabrera, A.; Hersey, A.; Leach, A. R. ChEMBL: Towards Direct Deposition of Bioassay Data. *Nucleic Acids Research* **2019**, *47* (D1), D930–D940. https://doi.org/10.1093/nar/gky1075.
(60) Ciriaco, F.; Gambacorta, N.; Leonetti, F.; Altomare, C. D.; Nicolotti, O. Virtual Reverse Screening Approach to Target Type 2 Cannabinoid Receptor. *Methods Mol Biol* **2023**, *2576*, 495–504. https://doi.org/10.1007/978-1-0716-2728-0_40.
(61) Farat, O. K.; Markov, V. I.; Varenichenko, S. A.; Dotsenko, V. V.; Mazepa, A. V. The Vilsmeier–Haack Formylation of 2,3-Dihydro-4H-1,3-Benzoxazin-4-Ones and Isomeric 1,2-Dihydro-4H-3,1-Benzoxazin-4-Ones: An Effective Approach to Functionalized 2H-/4H-Chromenes and Tetrahydroacridines. *Tetrahedron* **2015**, *71* (34), 5554–5561. https://doi.org/10.1016/j.tet.2015.06.069.
(62) Catani, V. M.; Gasperi, V. Assay of CB1 Receptor Binding. In *Endocannabinoid Signaling: Methods and Protocols*; Maccarrone, M., Ed.; Methods in Molecular Biology; Springer: New York, NY, 2016; pp 41–55. https://doi.org/10.1007/978-1-4939-3539-0_5.
(63) Caffarel, M. M.; Andradas, C.; Mira, E.; Pérez-Gómez, E.; Cerutti, C.; Moreno-Bueno, G.; Flores, J. M.; García-Real, I.; Palacios, J.; Mañes, S.; Guzmán, M.; Sánchez, C. Cannabinoids Reduce ErbB2-Driven Breast Cancer Progression through Akt Inhibition. *Molecular Cancer* **2010**, *9* (1), 196. https://doi.org/10.1186/1476-4598-9-196.
(64) Showalter, V.; Compton, D. R.; Martin, B.; Abood, M. Evaluation of Binding in a Transfected Cell Line Expressing a Peripheral Cannabinoid Receptor (CB2): Identification of Cannabinoid

Receptor Subtype Selective Ligands. *The Journal of pharmacology and experimental therapeutics* **1996**.
(65) Moreno, E.; Andradas, C.; Medrano, M.; Caffarel, M. M.; Pérez-Gómez, E.; Blasco-Benito, S.; Gómez-Cañas, M.; Pazos, M. R.; Irving, A. J.; Lluís, C.; Canela, E. I.; Fernández-Ruiz, J.; Guzmán, M.; McCormick, P. J.; Sánchez, C. Targeting CB2-GPR55 Receptor Heteromers Modulates Cancer Cell Signaling*. *Journal of Biological Chemistry* **2014**, *289* (32), 21960–21972. https://doi.org/10.1074/jbc.M114.561761.
(66) Tomko, A.; O'Leary, L.; Trask, H.; Achenbach, J. C.; Hall, S. R.; Goralski, K. B.; Ellis, L. D.; Dupré, D. J. Antitumor Activity of Abnormal Cannabidiol and Its Analog O-1602 in Taxol-Resistant Preclinical Models of Breast Cancer. *Frontiers in Pharmacology* **2019**, *10*.
(67) Ren, H.; Hu, D.; Mao, Y.; Su, X. Identification of Genes with Prognostic Value in the Breast Cancer Microenvironment Using Bioinformatics Analysis. *Medical Science Monitor* **2020**, *26*, e920212-1-e920212-12. https://doi.org/10.12659/MSM.920212.
(68) Danforth, D. N. The Role of Chronic Inflammation in the Development of Breast Cancer. *Cancers (Basel)* **2021**, *13* (15), 3918. https://doi.org/10.3390/cancers13153918.
(69) Geng, Y.; Chandrasekaran, S.; Hsu, J.-W.; Gidwani, M.; Hughes, A. D.; King, M. R. Phenotypic Switch in Blood: Effects of Pro-Inflammatory Cytokines on Breast Cancer Cell Aggregation and Adhesion. *PLOS ONE* **2013**, *8* (1), e54959. https://doi.org/10.1371/journal.pone.0054959.
(70) Chen, K.; Satlof, L.; Stoffels, G.; Kothapalli, U.; Ziluck, N.; Lema, M.; Poretsky, L.; Avtanski, D. Cytokine Secretion in Breast Cancer Cells – MILLIPLEX Assay Data. *Data in Brief* **2020**, *28*, 104798. https://doi.org/10.1016/j.dib.2019.104798.
(71) Ben-Baruch, A. Tumor Necrosis Factor α: Taking a Personalized Road in Cancer Therapy. *Frontiers in Immunology* **2022**, *13*.
(72) Sugiura, R.; Satoh, R.; Takasaki, T. ERK: A Double-Edged Sword in Cancer. ERK-Dependent Apoptosis as a Potential Therapeutic Strategy for Cancer. *Cells* **2021**, *10* (10), 2509. https://doi.org/10.3390/cells10102509.
(73) Romero-Sandoval, E. A.; Horvath, R.; Landry, R. P.; DeLeo, J. A. CANnabinoid Receptor Type 2 Activation Induces a Microglial Anti-Inflammatory Phenotype and Reduces Migration via MKP Induction and ERK Dephosphorylation. *Molecular Pain* **2009**, *5*, 1744-8069-5–25. https://doi.org/10.1186/1744-8069-5-25.
(74) Almeida, C. F.; Teixeira, N.; Correia-da-Silva, G.; Amaral, C. Cannabinoids in Breast Cancer: Differential Susceptibility According to Subtype. *Molecules* **2022**, *27* (1), 156. https://doi.org/10.3390/molecules27010156.
(75) Lee, X. C.; Werner, E.; Falasca, M. Molecular Mechanism of Autophagy and Its Regulation by Cannabinoids in Cancer. *Cancers* **2021**, *13* (6), 1211. https://doi.org/10.3390/cancers13061211.
(76) Gasperi, V.; Evangelista, D.; Oddi, S.; Florenzano, F.; Chiurchiù, V.; Avigliano, L.; Catani, M. V.; Maccarrone, M. Regulation of Inflammation and Proliferation of Human Bladder Carcinoma Cells by Type-1 and Type-2 Cannabinoid Receptors. *Life Sciences* **2015**, *138*, 41–51. https://doi.org/10.1016/j.lfs.2014.09.031.
(77) Alenabi, A.; Malekinejad, H. Cannabinoids Pharmacological Effects Are beyond the Palliative Effects: CB2 Cannabinoid Receptor Agonist Induced Cytotoxicity and Apoptosis in Human Colorectal Cancer Cells (HT-29). *Molecular and Cellular Biochemistry* **2021**, *476* (9), 3285–3301. https://doi.org/10.1007/s11010-021-04158-6.
(78) Allister, S. D. M.; Chan, C.; Taft, R. J.; Luu, T.; Abood, M. E.; Moore, D. H.; Aldape, K.; Yount, G. Cannabinoids Selectively Inhibit Proliferation and Induce Death of Cultured Human Glioblastoma Multiforme Cells. *Journal of Neurooncology* **2005**, *74* (1), 31–40. https://doi.org/10.1007/s11060-004-5950-2.
(79) Friesner, R. A.; Murphy, R. B.; Repasky, M. P.; Frye, L. L.; Greenwood, J. R.; Halgren, T. A.; Sanschagrin, P. C.; Mainz, D. T. Extra Precision Glide: Docking and Scoring Incorporating a

Model of Hydrophobic Enclosure for Protein−Ligand Complexes. *Journal of Medicinal Chemistry* **2006**, *49* (21), 6177–6196. https://doi.org/10.1021/jm051256o.
(80) Hua, T.; Li, X.; Wu, L.; Iliopoulos-Tsoutsouvas, C.; Wang, Y.; Wu, M.; Shen, L.; Brust, C. A.; Nikas, S. P.; Song, F.; Song, X.; Yuan, S.; Sun, Q.; Wu, Y.; Jiang, S.; Grim, T. W.; Benchama, O.; Stahl, E. L.; Zvonok, N.; Zhao, S.; Bohn, L. M.; Makriyannis, A.; Liu, Z.-J. Activation and Signaling Mechanism Revealed by Cannabinoid Receptor-Gi Complex Structures. *Cell* **2020**, *180* (4), 655-665.e18. https://doi.org/10.1016/j.cell.2020.01.008.
(81) Xing, C.; Zhuang, Y.; Xu, T.-H.; Feng, Z.; Zhou, X. E.; Chen, M.; Wang, L.; Meng, X.; Xue, Y.; Wang, J.; Liu, H.; McGuire, T. F.; Zhao, G.; Melcher, K.; Zhang, C.; Xu, H. E.; Xie, X.-Q. Cryo-EM Structure of the Human Cannabinoid Receptor CB2-Gi Signaling Complex. *Cell* **2020**, *180* (4), 645-654.e13. https://doi.org/10.1016/j.cell.2020.01.007.
(82) Lindahl; Abraham; Hess; Spoel, van der. GROMACS 2020.6 Manual. **2021**. https://doi.org/10.5281/zenodo.4576060.
(83) Li, X.; Hua, T.; Vemuri, K.; Ho, J.-H.; Wu, Y.; Wu, L.; Popov, P.; Benchama, O.; Zvonok, N.; Locke, K.; Qu, L.; Han, G. W.; Iyer, M. R.; Cinar, R.; Coffey, N. J.; Wang, J.; Wu, M.; Katritch, V.; Zhao, S.; Kunos, G.; Bohn, L. M.; Makriyannis, A.; Stevens, R. C.; Liu, Z.-J. Crystal Structure of the Human Cannabinoid Receptor CB2. *Cell* **2019**, *176* (3), 459-467.e13. https://doi.org/10.1016/j.cell.2018.12.011.
(84) Brennecke, B.; Gazzi, T.; Atz, K.; Fingerle, J.; Kuner, P.; Schindler, T.; Weck, G. de; Nazaré, M.; Grether, U. Cannabinoid Receptor Type 2 Ligands: An Analysis of Granted Patents since 2010. *Pharmaceutical Patent Analyst* **2021**, *10* (3), 111–163. https://doi.org/10.4155/ppa-2021-0002.
(85) Soethoudt, M.; Grether, U.; Fingerle, J.; Grim, T. W.; Fezza, F.; de Petrocellis, L.; Ullmer, C.; Rothenhäusler, B.; Perret, C.; van Gils, N.; Finlay, D.; MacDonald, C.; Chicca, A.; Gens, M. D.; Stuart, J.; de Vries, H.; Mastrangelo, N.; Xia, L.; Alachouzos, G.; Baggelaar, M. P.; Martella, A.; Mock, E. D.; Deng, H.; Heitman, L. H.; Connor, M.; Di Marzo, V.; Gertsch, J.; Lichtman, A. H.; Maccarrone, M.; Pacher, P.; Glass, M.; van der Stelt, M. Cannabinoid CB2 Receptor Ligand Profiling Reveals Biased Signalling and Off-Target Activity. *Nature Communication* **2017**, *8* (1), 13958. https://doi.org/10.1038/ncomms13958.
(86) Vale, N.; Silva, S.; Duarte, D.; Crista, D. M. A.; Silva, L. P. da; Silva, J. C. G. E. da. Normal Breast Epithelial MCF-10A Cells to Evaluate the Safety of Carbon Dots. *RSC Medicinal Chemistry* **2021**, *12* (2), 245–253. https://doi.org/10.1039/D0MD00317D.
(87) Sibilano, M.; Tullio, V.; Adorno, G.; Savini, I.; Gasperi, V.; Catani, M. V. Platelet-Derived MiR-126-3p Directly Targets AKT2 and Exerts Anti-Tumor Effects in Breast Cancer Cells: Further Insights in Platelet-Cancer Interplay. *International Journal of Molecular Sciences* **2022**, *23* (10), 5484. https://doi.org/10.3390/ijms23105484.
(88) Schrödinger Release 2020-4: Prime, Schrödinger, LLC, New York, NY, 2020.
(89) Schrödinger Release 2020-4: Protein Preparation Wizard; Epik, Schrödinger, LLC, New York, NY, 2016; Impact, Schrödinger, LLC, New York, NY, 2016; Prime, Schrödinger, LLC, New York, NY, 2020.
(90) Madhavi Sastry, G.; Adzhigirey, M.; Day, T.; Annabhimoju, R.; Sherman, W. Protein and Ligand Preparation: Parameters, Protocols, and Influence on Virtual Screening Enrichments. *Journal of Computer Aided Molecular Design* **2013**, *27* (3), 221–234. https://doi.org/10.1007/s10822-013-9644-8.
(91) Ballesteros, J. A.; Weinstein, H. [19] Integrated Methods for the Construction of Three-Dimensional Models and Computational Probing of Structure-Function Relations in G Protein-Coupled Receptors. In *Methods in Neurosciences*; Sealfon, S. C., Ed.; Receptor Molecular Biology; Academic Press, 1995; Vol. 25, pp 366–428. https://doi.org/10.1016/S1043-9471(05)80049-7.
(92) Schrödinger Release 2020-4: LigPrep, Schrödinger, LLC, New York, NY, 2020.

(93) Brooks, B. R.; Brooks III, C. L.; Mackerell Jr., A. D.; Nilsson, L.; Petrella, R. J.; Roux, B.; Won, Y.; Archontis, G.; Bartels, C.; Boresch, S.; Caflisch, A.; Caves, L.; Cui, Q.; Dinner, A. R.; Feig, M.; Fischer, S.; Gao, J.; Hodoscek, M.; Im, W.; Kuczera, K.; Lazaridis, T.; Ma, J.; Ovchinnikov, V.; Paci, E.; Pastor, R. W.; Post, C. B.; Pu, J. Z.; Schaefer, M.; Tidor, B.; Venable, R. M.; Woodcock, H. L.; Wu, X.; Yang, W.; York, D. M.; Karplus, M. CHARMM: The Biomolecular Simulation Program. *Journal of Computational Chemistry* **2009**, *30* (10), 1545–1614. https://doi.org/10.1002/jcc.21287.

(94) Jo, S.; Kim, T.; Iyer, V. G.; Im, W. CHARMM-GUI: A Web-Based Graphical User Interface for CHARMM. *Journal of Computational Chemistry* **2008**, *29* (11), 1859–1865. https://doi.org/10.1002/jcc.20945.

(95) Frisch G. W.; Schlegel, H. B.; Scuseria, G. E.; Robb, M. A.; Cheeseman, J. R.; Scalmani, G.; Barone, V.; Petersson, G. A.; Nakatsuji, H.; Li, X.; Caricato, M.; Marenich, A. V.; Bloino, J.; Janesko, B. G.; Gomperts, R.; Mennucci, B.; Hratch, D. J., M. J. . T. Gaussian 16, Rev. B.01. Gaussian, Inc., Wallingford, CT 2016].

(96) Bayly, C. I.; Cieplak, P.; Cornell, W.; Kollman, P. A. A Well-Behaved Electrostatic Potential Based Method Using Charge Restraints for Deriving Atomic Charges: The RESP Model. *Journal of Physical Chemistry* **1993**, *97* (40), 10269–10280. https://doi.org/10.1021/j100142a004.

(97) Wang, J.; Wang, W.; Kollman, P. A.; Case, D. A. Automatic Atom Type and Bond Type Perception in Molecular Mechanical Calculations. *Journal of Molecular Graphics and Modelling* **2006**, *25* (2), 247–260. https://doi.org/10.1016/j.jmgm.2005.12.005.

(98) Darden, T.; York, D.; Pedersen, L. Particle Mesh Ewald: An N·log(N) Method for Ewald Sums in Large Systems. *J. Chem. Phys.* **1993**, *98* (12), 10089–10092. https://doi.org/10.1063/1.464397.

(99) Hess, B.; Bekker, H.; Berendsen, H. J. C.; Fraaije, J. G. E. M. LINCS: A Linear Constraint Solver for Molecular Simulations. *Journal of Computational Chemistry* **1997**, *18* (12), 1463–1472. https://doi.org/10.1002/(SICI)1096-987X(199709)18:12<1463::AID-JCC4>3.0.CO;2-H.

(100) Bussi, G.; Donadio, D.; Parrinello, M. Canonical Sampling through Velocity Rescaling. *Journal of Chemical Physics* **2007**, *126* (1), 014101. https://doi.org/10.1063/1.2408420.

(101) Parrinello, M.; Rahman, A. Polymorphic Transitions in Single Crystals: A New Molecular Dynamics Method. *Journal of Applied Physics* **1981**, *52* (12), 7182–7190. https://doi.org/10.1063/1.328693.

(102) The UniProt Consortium. Reorganizing the Protein Space at the Universal Protein Resource (UniProt). *Nucleic Acids Research* **2012**, *40* (D1), D71–D75. https://doi.org/10.1093/nar/gkr981.

(103) Waterhouse, A. M.; Procter, J. B.; Martin, D. M. A.; Clamp, M.; Barton, G. J. Jalview Version 2—a Multiple Sequence Alignment Editor and Analysis Workbench. *Bioinformatics* **2009**, *25* (9), 1189–1191. https://doi.org/10.1093/bioinformatics/btp033.

1586 **Table of Contents Graphic**

1587

Exploring the 1,3-Benzoxazine Chemotype for Cannabinoid Receptor 2 as a Promising Anti-Cancer Therapeutic

Nicola Gambacorta, Valeria Gasperi, Tatiana Guzzo, Francesco Saverio Di Leva, Fulvio Ciriaco, Cristina Sanchez, Valentina Tullio, Diego Rozzi, Luciana Marinelli, Alessandra Topai, Orazio Nicolotti and Mauro Maccarrone

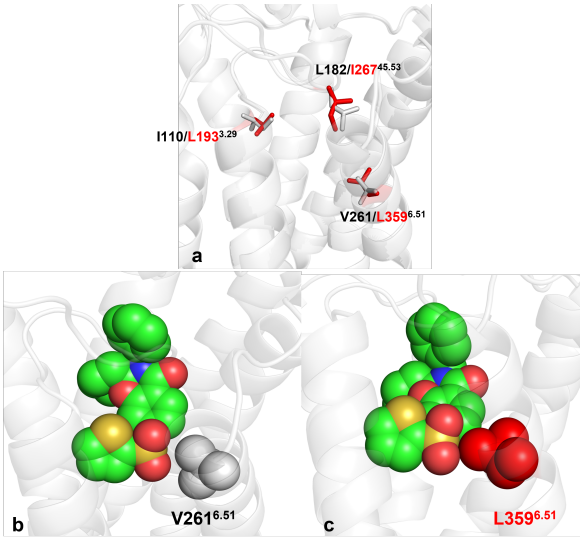

1588